

Debris disks around Sun-like stars

D. E. Trilling¹, G. Bryden², C. A. Beichman², G. H. Rieke¹, K. Y. L. Su¹, J. A. Stansberry¹, M. Blaylock¹, K. R. Stapelfeldt², J. W. Beeman³, & E. E. Haller^{3,4}

ABSTRACT

We have observed nearly 200 FGK stars at 24 and 70 microns with the *Spitzer* Space Telescope. We identify excess infrared emission, including a number of cases where the observed flux is more than 10 times brighter than the predicted photospheric flux, and interpret these signatures as evidence of debris disks in those systems. We combine this sample of FGK stars with similar published results to produce a sample of more than 350 main sequence AFGKM stars. The incidence of debris disks is $4.2^{+2.0}_{-1.1}\%$ at 24 microns for a sample of 213 Sun-like (FG) stars and $16.4^{+2.8}_{-2.9}\%$ at 70 microns for 225 Sun-like (FG) stars. We find that the excess rates for A, F, G, and K stars are statistically indistinguishable, but with a suggestion of decreasing excess rate toward the later spectral types; this may be an age effect. The lack of strong trend among FGK stars of comparable ages is surprising, given the factor of 50 change in stellar luminosity across this spectral range. We also find that the incidence of debris disks declines very slowly beyond ages of 1 billion years.

Subject headings: circumstellar matter — planetary systems: formation — infrared: stars

1. Introduction

Planetary system formation must be studied through various indirect means due to the relative faintness of distant planets and the long timescales over which planetary system

¹Steward Observatory, 933 N. Cherry Avenue, The University of Arizona, Tucson, AZ 85721; trilling@as.arizona.edu

²Jet Propulsion Laboratory, Caltech, 4800 Oak Grove Drive, Pasadena, CA 91109

³Materials Science Division, Lawrence Berkeley National Laboratory, Berkeley, CA 94720

⁴Department of Materials Science and Engineering, University of California, Berkeley, Berkeley, CA 94720

evolution takes place. One powerful technique has advanced substantially in the era of the *Spitzer* Space Telescope: investigations of dusty debris disks around mature, main sequence stars. Debris disks arise from populations of planetesimals that remain from the era of planet formation; the analogs in our Solar System are the asteroid belt and the Kuiper Belt. Any system that possesses a debris disk necessarily has progressed toward forming a planetary system to some degree.

The many small bodies that inhabit a debris disk can, on occasion, collide, producing a shower of fragments that grind each other down to dust particles. These dust grains can be heated by the central star to temperatures ~ 100 K, where they can be detected at wavelengths of 10–100 microns. Data from the IRAS and ISO satellites were used to identify and characterize debris disks (e.g., Aumann et al. 1984; Decin et al. 2000; Spangler et al. 2001; Habing et al. 2001; Decin et al. 2003). The Multiband Imaging Photometer for *Spitzer* (MIPS; Rieke et al. (2004)) offers substantially improved sensitivities at 24 and 70 microns and therefore can be used to advance the study of debris disks and measure the fraction of stars that possess colliding swarms of remnant planetesimals.

A number of these surveys have been carried out using MIPS. Rieke et al. (2005) and Su et al. (2006) observed hundreds of A stars and found that the number of A stars showing thermal infrared excess suggestive of collisionally-produced dust decreases as a function of stellar age, from 50% or more at ages just past the gas dissipation age of 10 Myr to 30% at 500 Myr. The excess rates are lower for older and lower mass stars. Bryden et al. (2006) found that the excess rate is around 15% for stars of mass and age similar to our Sun (for a sample of 69 stars). Gautier et al. (2007) did not detect any 24 or 70 micron excesses suggestive of debris disks in a sample of 60 field (old) M stars (with only 13 strongly detected at 70 microns). Finally, multiplicity appears to play a significant role in modulating debris disks, as Trilling et al. (2007) found that the debris disk rate for A and F binaries was higher than that for single stars of similar spectral types.

We present here a survey for excesses around almost 200 F, G, and K stars, with ages and masses similar to that of our Sun. (Some of these data were published in Bryden et al. (2006).) We characterize the excesses that we find and present a few systems of particular interest. We create a larger sample of FGK stars by adding 75 stars from a similar survey, and derive excess rates as a function of spectral type and as a function of age. Finally, we discuss the implications of our results for planetary system formation.

2. Sample selection

The data presented here originate in two separate observing programs. The majority are from a survey targeting nearby late F, G, and early K “Solar type” stars (*Spitzer* GTO program #41). Results for 69 stars from this program were published in Bryden et al. (2006) (hereafter B06), and the present paper completes the analysis of data from that program. For completeness, all targets that appeared in B06 are also included in this paper. The remainder of the data belong to a survey for debris disks among F stars (*Spitzer* GTO program #30211). Stars in this spectral type range were omitted from previous *Spitzer* disk surveys, and have particular relevance in determining the nature of the transition from the high A star debris disk incidence to the more modest incidence for Sun-like stars. Furthermore, these 49 F stars will serve as a useful control sample to the Trilling et al. (2007) result that binary A and F stars have a relatively high excess rate. We combine the data from these two samples here to give continuous coverage, a large sample of stars, and overall view of debris disks from F0 to K5 stars. We refer to the combined sample of 193 stars (PID 41 plus PID 30211) as our FGK sample. Relevant information for the combined target list is given in Table 1. Figures 1–4 show the distributions of targets as functions of spectral type, distance, age, and metallicity.

2.1. F stars sample

Our target list was assembled in the following way. A list of main sequence F0–F5 stars was created from the Hipparcos database, in order of increasing distance from the Earth. All stars that were known to be members of multiple systems were removed (by vetting against the CCDM catalog). Next, systems that were obviously young (less than 1 Gyr) were removed, using the measurements of Nordstrom et al. (2004). The average age of our sample is around 3 Gyr (compare to the average age of the “Solar type” FGK sample presented in Section 2.2 of around 5 Gyr). We used the IPAC IBIS tool to extract the infrared background and confusion levels from the IRAS data for each remaining target, compared the predicted target photospheric flux to the confusion per MIPS beam, and discarded targets with predicted $S/N < 3$. Finally, we discarded targets requiring 70 micron integration times longer than 1300 second (12 cycles of 10 second integrations); targets fainter than this rapidly become very expensive with questionable return. These selection criteria left 49 targets as our final target list. Here we present the 37 of those targets observed to date; the remaining stragglers will be published in a future paper.

2.2. “Solar type” sample

The “Solar type” sample selection is described in detail in B06. We briefly summarize that description here. This program consists of two overlapping sets of stars: those that meet strict selection criteria for an unbiased sample, and those that are known to harbor planets. In both cases, only stars with spectral type similar to the Sun are considered. Stars with spectral type F5 to K5 and luminosity class IV or V were included, with the final list chosen by expected signal to noise ratio for photospheric flux. Additionally, a minimum photospheric 70 micron flux was set for each spectral type bin: 20 mJy for F5-F9 stars, 10 mJy for G0-G4, and 5 mJy for G5-K5. There is no explicit selection based on stellar age or metallicity; however, the 70 micron brightness and S/N thresholds are relaxed in some cases to allow stars with well determined ages into the sample. Close, resolved binary systems are excluded. The total sample presented here is 156 stars (non-planet stars and planet stars, combined). A companion paper (Bryden et al. 2007) describes the planet-bearing sample in more detail.

3. Observations and data reduction

A listing of the observations for these programs is given in Table 2. All *Spitzer* observations reported here were made between January, 2004, and March, 2007. We used MIPS to observe each system at 24 μm and 70 μm (effective wavelengths 23.68 and 71.42 μm , respectively). All stars were observed in MIPS Photometry small-field mode. The 24 μm observations all used 3 sec DCEs (data collection events) and a single template cycle (with a few exceptions; see Table 2). The 70 μm observations typically used 10 sec DCEs and 5 to 10 template cycles.

Overall, our data analysis is similar to that previously described in Beichman et al. (2005a), Bryden et al. (2006), and Beichman et al. (2006b). The data reduction is based on the DAT software developed by the MIPS instrument team (Gordon et al. 2005). At 24 microns, image flats are chosen as a function of scan mirror position to correct for dust spots (Engelbracht et al. 2007a). Images were mosaicked from individual frames with half-pixel subsampling. We carried out aperture photometry on reduced images as described in Beichman et al. (2005a), using an aperture of six $2''.55$ pixels, a sky annulus of 12–17 pixels, a calibration factor of $1.047 \mu\text{Jy}/\text{arcsec}^2/(\text{DN}/\text{s})$, and an aperture correction of 1.15. At 70 microns we used images processed beyond the standard DAT software to correct for time-dependent transients, corrections that can significantly improve the sensitivity of the measurements (Gordon et al. 2007). Because the accuracy of the 70 micron data is limited by background noise, rather than instrumental effects, a very small photometric aperture was

used to maximize signal-to-noise – just 1.5 pixels in radius, requiring an aperture correction of 1.79. An annulus with an inner radius of 4 pixels and an outer radius of 8 pixels was used to measure the sky background around each target. The flux level is calibrated at 16.5 mJy/arcsec²/MIPS_70_unit, with a default color correction of 1.00 (MIPS_70_units are based on the ratio of the measured signal to the stimulator flash signal). For both the 24 and 70 micron data, neighboring point sources were subtracted from the images before measuring the sky brightness.

The 24 micron centroid positions, which are consistent with the telescope pointing accuracy of <1" (Werner et al. 2004), are used as the target coordinates for both wavelengths. The only significant update from previous papers is a 4% increase in the overall calibration at 70 microns from 15.8 to 16.5 mJy/arcsec²/MIPS_70_unit.

4. Photospheric predictions and detections of excess

4.1. 24 μm

To determine whether any of our target stars have an IR excess, we compare the measured photometry (F) to predicted photospheric levels (P). High quality K magnitudes are required to extrapolate to 24 microns. Most of our stars have good 2MASS photometry (Skrutskie et al. 2006), but stars brighter than $m_K \sim 4.5$ saturate in 2MASS and therefore this survey cannot provide accurate photometry. We obtained photometry for as many of these “non-2MASS” stars as possible from the literature, and transformed it to the 2MASS system according to relations in Bessell et al. (1998) and Carpenter (2001). The errors for some of this “heritage photometry” are difficult to estimate, since infrared photometric systems were still under evolution when some of it was obtained. We show below that the net errors after transformation are surprisingly small. For 16 additional stars where we could find no K-band photometry, we estimated values from B-I or B-V colors. We obtained the optical colors from SIMBAD for the members of our sample and carried out linear fits against I-K or V-K. The rms scatter around the fit was 0.07 for B-I vs. I-K and 0.09 for B-V vs. V-K, and we take this scatter to be the error in the estimated K and K_S magnitudes. There are 12 stars for which we were unable to make even estimates of K and K_S magnitudes.

For the 181 sources where K_S data is available, we use the following approach. We computed ratios of the measured flux densities at 24 microns and K_S to determine the mean photospheric color. There is a weak dependence of this photospheric color on spectral type. We calculated this correction by assigning a numerical value proportional to spectral type (0 for A0, 10 for F0, 15 for F5, etc.) and multiplying the ratios by $1.048/(1+0.048*(\text{type}/22))$,

determined from a linear fit to the data. This procedure results in a predicted 24 micron flux (P24) for each of these 181 stars.

We then calculate the excess ratios ($R_{24}=F_{24}/P_{24}$) for each system (Table 3). The distribution of derived excess ratios is shown in Figure 5. The R_{24} distribution for all stars with K_S magnitudes (2MASS or heritage) is quite regular, with clear peak near unity. For $0.92 \leq R_{24} \leq 1.08$, the mean and median both have a value of 0.995, with an rms scatter of 0.032. For only the stars with heritage photometry, the analogous average is 0.997, the rms scatter is 0.031, and the median is 0.999. That is, there is no evidence for any systematic difference in the sources of K photometry and we can treat all stars measured in this way identically. We can therefore set a 3σ threshold for identification of an excess. Our approach is the same that we took in Su et al. (2006). We take 1σ to be the rms scatter value of 0.032. Our result of zero sources with $R_{24} < 0.92$ is consistent with this value of σ . We therefore set the 3σ excess threshold to be 1.10. One star (HD 222404) has $R_{24}=1.10$, and we consider this marginal case explicitly in the next paragraph. The next smallest R_{24} value above our 3σ threshold is 1.15 (close to 5σ), and six stars have even larger R_{24} values. The stars with 2MASS K_S magnitudes or heritage K magnitudes and excesses at $24\mu\text{m}$ are HD 166, 3126, 69830, and 105912.

The stars with possible excesses based on estimated K magnitudes need to be discussed individually because of their larger K magnitude uncertainties. HD 10647 has a ratio of 1.21, based on extrapolation from B-V and hence at a level of $\sim 2.5\sigma$. It has a very large excess at $70\mu\text{m}$, by more than a factor of ten over the photosphere, and Chen et al. (2006) find an excess at 30–34 microns, so we consider the excess at $24\mu\text{m}$ to be confirmed at the longer wavelengths. HD 101259 has an indicated excess ratio of 1.25, based on extrapolation from B-V, and hence at nearly 3σ . It is not saturated in the 2MASS data at J, and if we apply the standard J-K color for its spectral type, we estimate an excess ratio of 1.15. It has a modest but significant excess at $70\mu\text{m}$, so we accept the reality of the indicated one at $24\mu\text{m}$. HD 191408 has a ratio of 1.23, based on an estimate from B-I and hence at a level of $\sim 3\sigma$. It has no significant excess at $70\mu\text{m}$, with a 2σ upper limit to the excess ratio of 1.7. We used Kurucz model fitting to make an independent prediction of the $24\mu\text{m}$ flux density, and found an excess ratio of only 1.08, suggesting that our extrapolation is in error, probably due to a bad photometric point. Furthermore, IRS spectra throughout this region are photospheric (no excess) (Beichman et al. 2006a). It is therefore unlikely that the possible $24\mu\text{m}$ excess is real. HD 222404 has an excess ratio of 1.10 based on a K magnitude estimated from B-I, and hence at a level of 1.5σ . However, the 2σ upper limit to the excess ratio at $70\mu\text{m}$ is only 1.04, so we reject the possibility of an excess at $24\mu\text{m}$. The remaining stars with estimated K magnitudes all have excess ratios < 1.10 . In summary, we therefore find six stars in the sample of stars with K magnitudes (2MASS, heritage, or estimated)

with significant 24 μm excesses (Table 5): HD 166, 3126, 10647, 69830, 101259, and 105912.

This “self calibration” technique (using the data to define the outliers) is generally required in determining intrinsic stellar colors. For extreme outliers (Figure 5), there is no question of the veracity of this technique. Furthermore, because the distribution of R24 is well-behaved, with very small scatter, we are confident that it robustly reflects the true distribution of excesses. We further note that there is no procedure other than self calibration that works. There is no sample of stars measured at 24 μm that includes the relevant spectral types and that is certain to have no small excesses. Kurucz model fitting leaves a small residual that must be removed empirically (Su et al. 2006). We checked our results using model fitting for a subset of targets and found agreement with the photometry-based extrapolations performed for the entire sample. Finally, we note that the rms scatter in the distribution of R24 is 0.02–0.023 from the K-band photometry, 0.01 from the 24 μm photometry, and about 0.01 from the color-color relationships. Assuming these errors add quadratically (they are independent errors), the error left for variations in stellar color is 0.019, a very small number. This leaves little room for significant excesses for the bulk of the stars. We conclude that our self calibration technique is robust.

4.2. 70 μm

Since the majority of the stars in our sample do not have 24 micron excesses, in general we make our 70 micron photospheric predictions based on the 24 micron flux measurements. For stars with no excess emission, the expected F24/F70 ratio is 9.10 (scaling by λ^2 and using the effective wavelengths specified above), so we derive predicted 70 micron fluxes by dividing the observed 24 micron fluxes by this numerical factor. The predicted fluxes (P70) are listed in Table 3. Calculating P70 this way (and not from extrapolations from K magnitudes) allows us to capitalize on the nearly uniform 24/70 flux ratio rather than extrapolating from K and potentially magnifying any slight misestimates. It also allows us to determine P70 for the 12 stars that have no K band measurements and therefore no P24, so that we can search all 193 stars in our sample for 70 micron excesses. Naturally, for the six stars with 24 micron excess this extrapolation from observed 24 micron fluxes to 70 micron predictions does not work; for these systems, we extrapolate the predicted 24 micron fluxes to derive predicted 70 micron fluxes, using this same numerical factor of 9.10. For these six cases, our 70 micron predictions are confirmed with Kurucz model fitting.

The large scatter and large number of (expected) excesses at 70 microns makes determining the excess threshold in the circular manner above problematic. We instead quantify the significance of the (possible) 70 micron excess χ_{70} , which is defined as follows:

$$\chi_{70} = \frac{F70 - P70}{\sigma_{70}}$$

where F70 and P70 are as defined above and σ_{70} is the error in the measurement.

We use the same criterion as Su et al. (2006) to identify significant excesses: we require $\chi_{70} \geq 3$. This is identical to saying that the significance of the excess must be at least 3σ . The distribution of χ_{70} is shown in Figure 6. The core of this distribution is clearly centered near zero, the expected value for a sample where non-excess is the majority outcome. Nevertheless, the distribution of χ_{70} shown in the top panel of Figure 6 is not symmetric in the range $-3 < \chi_{70} < 3$: the broad shape of the right “shoulder” in the top panel of Figure 6 ($1.5 < \chi_{70} < 3$) suggests the presence of a number of low-level excesses (below our detection threshold).

In our large sample, we can test the reliability of these determinations by counting the number of stars that fall below our -3σ excess criteria (that is, $\chi_{70} \leq -3.0$). Only one star (HD 100067) has $\chi_{70} \leq -3.0$ (Figure 6). This system has a large negative χ_{70} value because the measured aperture photometry is formally negative (meaning the sky value subtracts more than the enclosed flux in the photometric aperture); in other words, this star was simply not detected at 70 microns (Table 3). There are no cases of $\chi_{70} < -3.0$ where the star is detected. Assuming symmetric noise properties, we therefore expect no spurious positive outliers.

In summary, we identify any system with $\chi_{70} \geq 3.0$ as an excess system. There are 27 such systems out of the 181 stars with K magnitudes. We define HD 69830 to have an excess at 70 microns because it has $\chi_{70} = 2.81$ and a significant (corroborating) excess at 24 microns (R24=1.47), bringing the number of systems with 70 micron excesses to 28 out of 181. This 28 includes 6 systems that have excesses at both 24 and 70 microns. Finally, 2 of the 12 stars with no K magnitudes also have 70 micron excesses (see Section 5.3), based on $F24/F70 < 9.10$. This brings the total number of systems with 70 micron excesses to 30 out of 193 (Table 3).

In Figure 7 we show the distribution of our 181 sources with K magnitudes in R24- χ_{70} space. We confirm that there are likely no other spurious 24 micron excesses. Furthermore, the random scatter distribution (fully uncorrelated) of the non-excess sources confirms that there are no systematic errors introduced by our technique of predicting 24 micron fluxes and extrapolating to predict 70 micron fluxes. Systems with weak excesses at both 24 and 70 microns would not necessarily be identified by the techniques we have described here. However, we see in Figure 7 that there are no systems in the upper right of the enclosed

area, where such a system with two weak excesses would reside.

5. Results

5.1. Excess rates

There are 181 stars in our sample with well-constrained K band magnitudes and therefore reliable 24 micron predicted fluxes. We can make excess determinations for all 193 stars at 70 microns (in most cases based on our 24 micron measurements). We add to this catalog three stars that meet the selection criteria for PID 41 but had already been included in other observing programs: ϵ Eri (K2V, 3×10^8 yr); τ Ceti (G8V, 7.2×10^9 yr); and τ^1 Eri (F6V, 3×10^8 yr) (Table 3 from B06 as well as Decin et al. (2003); Chen et al. (2006)). The first of these has excesses at both 24 and 70 microns (Backman et al., in prep.); the second is photospheric at 24 microns and has an excess at 70 microns (Chen et al. 2006; Stapelfeldt et al. 2006); and the third has no excess at either 24 or 70 microns (Chen et al. 2006; Stapelfeldt et al. 2006; Trilling et al. 2007). These additions bring the total excess rates to the following values: at 24 microns, 7 out of 184 stars have excesses, giving $3.8_{-1.2}^{+1.7}\%$; and at 70 microns, 32 out of 196 stars have excesses, giving $16.3_{-2.8}^{+2.9}\%$. In all cases in this paper, we cite binomial errors that include 68% of the probability (equivalent to the 1σ range for gaussian errors), as defined in Burgasser et al. (2003). All of the systems with 24 micron excesses also have 70 micron excesses. These excess rates are also presented in Table 4.

Of the 196 stars presented here in our FGK sample, 48 are known to harbor extrasolar planets. The excess rates for the planet sample are higher than the no-planet sample, although formally the two samples' excess rates are consistent at the 1σ level (Table 4). Bryden et al. (2007) discuss further the differences for excess rates and debris disks for stars with and without known planets. Planets have been found around $\sim 10\%$ of the stars surveyed in radial velocity programs (Udry et al. 2007), but here planet-bearing stars represent 25% of the total FGK sample, so there is the potential for contamination of our derived excess rate for FGK stars. However, if we weight the planets and no-planets excess rates (Table 4) by 10% and 90%, respectively, we find that the resulting total excess rates are 3.9% (24 microns) and 15.6% (70 microns), hardly different from the overall excess rates derived above ($3.8_{-1.2}^{+1.7}\%$ and $16.3_{-2.8}^{+2.9}\%$, respectively). We conclude that any contamination must therefore be insignificant.

5.2. Dust properties

We interpret the presence of excess thermal infrared flux as a signature of emission from dust grains. These dust grains are assumed to be produced relatively recently from collisions of asteroid-like bodies. (Dust grains in these systems have short lifetimes against radiation forces.) By constraining the properties of this dust, we can learn about the processes of planetary system formation in a large sample of FGK stars.

In general, we would like to fit the observed excesses to a black body to determine the temperature of the excess. For systems with excesses at both 24 and 70 microns this is relatively straightforward: we find the blackbody temperature that best fits the two observed excesses. These temperatures are given in Table 5. We scale this blackbody by the appropriate amount to fit the excess measurements. The ratio of this scaled blackbody’s integrated flux to the star’s integrated flux is the fractional luminosity (Table 5, Figure 8).

Most stars in our sample that show excesses, however, have excesses only at 70 microns, which leaves dust temperatures relatively unconstrained. In these cases — excess flux at 70 microns, photospheric flux at 24 microns — we set the 24 micron “excess” to be equal to three times the error at 24 microns (which is dominated by the calibration uncertainty), and find the blackbody that best fits this “excess” and the measured 70 microns excess. This resulting temperature is the maximum temperature for the excess (Table 6).

After solving for this dust temperature (T_d), we can calculate the orbital distance r (in AU) of the dust through equation 3 from Backman & Paresce (1993):

$$r = \left(\frac{278}{T_d}\right)^2 \left(\frac{L_\star}{L_\odot}\right)^{0.5} \quad (1)$$

where L_\star is the stellar luminosity. (Large grains with unit emissivities that radiate as black bodies are assumed.) We calculate the stellar luminosity of the host star simply through

$$L_\star = 4\pi R_\star^2 \int \text{Kurucz model} = 4\pi R_\star^2 \sigma T_{eff}^4 \quad (2)$$

where R_\star is the stellar radius (from Drilling & Landolt 2000) and the stellar effective temperature T_{eff} is given in Table 1 and again in Table 6. Our calculated dust distances are given in Tables 5 and 6 and Figure 8. For systems with excesses only at 70 microns, the distances we derive are minimum distances, since the dust temperatures we derive are maximum temperatures. In all cases, we assume black body grains.

Finally, from our blackbody fits to the excesses we also derive the fractional luminosities:

the ratios of dust luminosity to stellar luminosity. This quantity is also referred to as f_d and L_d/L_* . The fractional luminosities we derive are given in Tables 5 and 6 and Figure 8. As above, for systems with excesses only at 70 microns, these derived fractional luminosities are the maximum values that are consistent with the observed data. However, extremely massive cold outer disks, which could imply a larger fractional luminosity than the “maximum” values we present here, cannot be ruled out.

To place a reasonable lower limit on the fractional luminosity estimates for systems with excesses only at 70 microns, we follow the arguments in B06 and Trilling et al. (2007) and assume a “minimum” possible disk temperature of 50 K. This assumption excludes the possibility that a very cold (and potentially massive) disk could exist, with emission at wavelengths longer than 70 microns. This 50 K blackbody is scaled to match the measured 70 micron excesses (this results in no detectable excess emission at 24 microns, consistent with the observations). We calculate the ratio of this disk’s luminosity to the stellar luminosity to derive the minimum fractional luminosities for systems with excesses at 70 microns only. We present these minimum disk luminosities in Table 6 and Figure 8. These two estimates of fractional luminosity give the range of values that fit the data. In many cases, the range of acceptable values is quite small. We see that the minimum fractional luminosity is around 10^{-5} , as has been found in other surveys as well (Bryden et al. 2006; Trilling et al. 2007).

5.3. Individual systems of interest

We describe here a few interesting individual cases, some of which are also shown in Figure 9, to demonstrate the range of disk properties evident in our sample.

HD 693. This system has $\chi_{70} = 2.95$, just below our excess threshold. It is likely that there is a real excess in this system that is simply slightly too faint for us to detect formally. Additionally, a massive and/or cold(er) disk cannot be ruled out. We identify this system as one of particular interest because of its low fractional luminosity: 3×10^{-6} (assuming that there is a real excess), which would make it comparable to some estimates of our Solar System’s Kuiper Belt (Figure 9). Also of note is its dust distance of 3.2 AU, clearly well within the realm of possible planetary systems.

HD 3126. This star has a very large 70 micron excess ($\chi_{70} = 35.8$) and a modest 24 micron excess ($R_{24}=1.16$). With an age of 3.5 Gyr and a SIMBAD spectral type of F2, there is nothing apparently anomalous about this system that could explain its large excess, i.e., the star is not young, nor is it evolved. (Favata et al. (1993) assign a spectral type of F4V.) In Figure 9, we show the narrow range of possible fractional luminosities ($\sim 10^{-4}$) that are in

accord with the observed data. The fractional luminosity is relatively high. This system is clearly promising for additional observations to better characterize the dust population.

HD 10647. This star has a well-known infrared excess that was first detected with IRAS (Stencel & Backman 1991). Chen et al. (2006) determined a fractional luminosity of 15×10^{-5} for this system with *Spitzer*/IRS measurements, using a temperature of 70 K. This is fairly consistent with the values we derive (Table 5), and is a relatively large fractional luminosity for the FGK sample we present here. HD 10647 is also known to harbor (at least) one extrasolar planet, orbiting at 2 AU (Butler et al. 2006). We find the dust to be at a distance of at least 21 AU (Table 5), although Jura et al. (2004) find an inner disk radius of 11 AU using IRS spectra and a warmer excess temperature than we find. This disk has also been detected in scattered light (Stapelfeldt et al., in prep.). This system is clearly fertile ground for further studies of planetary system formation, since both a giant planet and a large dust disk (and implied collisions among asteroidal bodies) are known to exist.

HD 19994. There is no good K magnitude for this system, so we cannot determine whether it has a 24 micron excess. However, F24/F70 is 5.6, making this system far too bright at 70 microns for the [24:70] color to be photospheric; we determine $\chi_{70} = 4.25$. This assumes that F24 is photospheric, which is the conservative assumption that makes our calculated χ_{70} a lower limit. Under this assumption, the maximum dust temperature is 170 K, the minimum dust distance is 4.1 AU, and the maximum fractional luminosity is 4×10^{-5} . These properties are similar to the other systems with excesses at 70 microns only.

HD 30495. Among systems with no 24 micron excesses, HD 30495 has the most significant 70 micron excess ($\chi_{70} = 26.9$). These parameters suggest a relatively cool dust disk, as seen in Figure 9. As for HD 3126, a massive, cold disk cannot be ruled out.

HD 69830. This system was discovered by Beichman et al. (2005b) to have substantial hot emission, which Lisse et al. (2007) attributed to the recent breakup of a large asteroid in that system. The excess infrared emission, evident from 8–35 microns (and, as we show here, marginally evident in photometry¹ at 70 microns), suggests quite high temperatures (~ 400 K) and a dust distance around 1 AU. This system further became interesting with the subsequent discovery of three Neptune mass planets in that system, all orbiting at less than 1 AU (Lovis et al. 2006).

¹The 70 micron flux reported here [26 mJy] is higher than that in Beichman et al. (2005b) [19 mJy] primarily due to better centering of the photometric aperture on the source. There is an additional small [5%] increase in the calibration factor that has been applied since Beichman et al. (2005b).

HD 82943. Among systems with excesses at 70 microns only, HD 82943 has the largest fractional luminosity, at more than 10^{-4} (Table 6). Moór et al. (2006) find that all systems with debris disk fractional luminosities greater than 5×10^{-4} are young. HD 82943 has an age of more than 4 Gyr (Table 1). Our fractional luminosity estimates for the disk around HD 82943 are below this apparent limit, so the age of more than 4 Gyr (Table 1) offers no direct contradiction. Nevertheless, this system may be useful in helping to define the exact border of the distribution discussed by Moór et al. (2006). (Other high fractional luminosity systems given in Tables 5 and 6 may also provide useful constraints.) We note that HD 82943 also has two planets orbiting it interior to 1.5 AU; these planets are locked in a 2:1 mean motion resonance (Mayor et al. 2004; Lee et al. 2006).

HD 101259. We find an excess at both 24 and 70 microns for this star. Unusually, the excess in this system is not much brighter, relatively, at 70 microns than at 24 microns ($R_{24}=1.25$ and $R_{70}=1.61$). However, we note that both P24 and P70 for this system are based on the B-V color, and therefore have a large uncertainty. Taken together, a small and warm excess is likely, but not certain. Follow-up observations will be critical in characterizing this system, and will be of particular interest since systems with warm dust are rare.

The measured excesses of $R_{24}=1.25$ and $R_{70}=1.61$ require a fairly warm disk temperature of 271 K, giving a dust distance of around 1 AU (Table 5). (The IRAS 12 micron flux also appears to be $\sim 25\%$ higher than the expected photospheric flux.) The properties of this disk appear quite similar to HD 69830 (see Figure 7), and further observations (including IRS spectroscopy) should be made to characterize the dust population. In temperature and distance, the dust in this system closely resembles the zodiacal dust in our Solar System, which is produced largely by collisions in the asteroid belt. The architecture of that planetesimal (and potential planet) system may not be that different from our own Solar System’s.

HD 207129. There is no good K magnitude measurement for this star, so we cannot predict its 24 or 70 micron fluxes. Nevertheless, this star has been known to have an infrared excess for more than 20 years (Aumann 1985), and has been studied with both ISO (Jourdain de Muizon et al. 1999) and in a number of ongoing *Spitzer* studies. The F24/F70 ratio of 0.57 that we observe here is far from the photospheric value of 9.10 and clearly indicates a strong 70 micron excess and presence of a debris disk. We fit published visible and near-infrared data with a Kurucz model to predict the 24 and 70 micron fluxes (Figure 10) and constrain the dust properties.

We find $P_{24}=139$ mJy and $P_{70}=15$ mJy. This gives excesses at 24 and 70 microns of 25 and 274 mJy, respectively. The fractional luminosity is around 10^{-4} , which is very high for a star like our Sun. The color temperature is 72 K, which, for this G0 star, gives R_{dust} of

15.3 AU. The temperature we derive is hotter than the ISO-derived range of 15–45 K, but our fractional luminosity agrees well with their values (Jourdain de Muizon et al. 1999). The properties we derive are similar to the other systems with excesses at both bands (Table 5). This debris disk ring has also been detected directly in scattered light (Krist et al., in prep.).

6. Discussion

6.1. Metallicity and excesses

Four stars in our FGK sample do not have published metallicities. For the 189 stars with known metallicities in Table 1, the mean metallicity is -0.08 ± 0.22 , with a median of -0.06 . The mean metallicity of stars with excesses is -0.11 ± 0.19 (median is -0.09). The mean metallicity of stars with no excesses is -0.08 ± 0.22 (median is -0.05). There is no difference between the metallicity of the population of stars with excesses and the population of stars with no excesses. This lack of correlation has been discussed previously (e.g., B06, Beichman et al. (2006b)).

6.2. Excess rates across spectral type

Many parameters affecting infrared excesses change with spectral type, including the importance of grain loss mechanisms (winds, Poynting-Robertson drag, photon pressure); stellar luminosity; and the locations of key temperatures (e.g., the ice line) in the systems. Significant surveys for debris disks across spectral types A–M have now been published, and we use those data to look for systematic trends across spectral types.

It is well known that excess rates decrease with stellar age (Habing et al. 2001; Spangler et al. 2001; Rieke et al. 2005; Su et al. 2006; Siegler et al. 2007). This dependence must be avoided in testing for changes with spectral type. We take the oldest (≥ 600 Myr) A stars from the Su et al. (2006) sample as our representative sample from that spectral type. For our F, G, and K samples we take the union of the data presented here and the data in Beichman et al. (2006b). The targets and data reduction presented in Beichman et al. (2006b) are quite similar to the selections and techniques we have employed here, which allows us to merge the two samples relatively seamlessly. We calculate the excess ratios for these F, G, and K samples and take the M stars excess rates from Gautier et al. (2007). This compilation is presented in Table 4 and Figure 11.

Within the error bars, the excess rates for the A, F, G, and K subsamples are essentially

indistinguishable. However, there is a suggestion of a trend of decreasing $70\ \mu\text{m}$ excess rates with later spectral types (Figure 11). We note, however, that the mean age for the populations increases with later spectral types. It is possible that we are instead detecting a time-related effect, although the decay timescales identified by Rieke et al. (2005), Su et al. (2006), and Siegler et al. (2007) of hundreds of millions of years should long since have diminished all disks at ages of billions of years. We discuss this possibility in Section 6.3.

Beichman et al. (2006b) remarked that the excess rates for K stars appeared to be lower than that for F and G stars, finding zero excesses among 23 stars later than K2 (and zero excesses among a larger combined sample of 61 K1–M6 stars). We include the Beichman et al. (2006b) data in our analysis here, and find that, formally, the excess rate for K stars is not significantly different than the excess rates for earlier (F and G) stars. As Beichman et al. (2006b) note, and we confirm, none of the 6 K stars with excesses in our larger sample are later than K2.

Part of the motivation for assembling the F stars program (PID 30211) was as a control sample for the binary star program presented in Trilling et al. (2007). In that study, 69 A3–F8 binary star systems were found, overall, to have relatively high excess rates: 9% at 24 microns and 40% at 70 microns. It is clear from our results here (see Figure 11) that the (single) F stars excess rate is equal to or lower than the (single) A stars excess rate. The binaries excess rates remain significantly high compared to the control sample of A and F stars.

Figure 8 shows that, in general, there is no trend of dust distance as a function of stellar effective temperature (spectral type). This may suggest that the processes that drive planetesimal formation do not depend strongly on a single critical temperature, as would be the case in the “ice line” model, where protoplanetary disk surface densities increase across certain temperature boundaries. However, our method for calculating dust distances may be too crude to see this effect. We note that all of the (minimum) dust distances given in Table 6 would fall within the planetary realm of our Solar System (<30 AU). We are not observing disks that are far outside of the potential planetary realm of these systems.

We stated above that there is no particular trend for either fractional luminosity or dust distance with spectral type, but there is an important caveat: no disks with large dust distances or relatively small fractional luminosities were identified among the latest stars in our sample. This dearth may simply allude to the fact that later stars are cooler. Dust at 25 AU around a K1 (5000 K) star would have a temperature around 50 K; this dust would have its peak emission near 70 microns, and cooler (more distant) dust would have its peak emission longward. MIPS 70 micron observations of such a dust population, or a cooler one, would not readily show the presence of this excess. The lack of distant disks around K stars

may therefore be an observational bias. Similarly, low fractional luminosity disks would be more difficult to detect around K stars than around earlier stars, so the lack of low fractional luminosity disks for later stars may also be due to observational bias. These observational biases may be corrected with sufficiently sensitive measurements at ~ 100 microns (e.g., with Herschel).

To further address the question of whether there is any detectable trend of excess rate as a function of spectral type using existing published data, we compared the incidence of $70 \mu\text{m}$ excesses across these 5 spectral types (A, F, G, K, M), a total sample size of more than 350 stars. To avoid uncontrolled selection effects, we confined the comparison to stars that would have been detected at 70 microns at a level of at least 2:1 on the photosphere. We then applied a number of tests. First, we computed weighted average values of R70 (observed flux over predicted flux) as in Gautier et al. (2007). We find a value of ~ 5 for the A stars, but we discount this large average because of the small size of the sample (27 stars). The values for the F, G, K, and M stars are 1.16, 1.23, 1.06, and 1.025, respectively. Errors are difficult to estimate because the excesses are not normally distributed. We also computed straight averages of R70 for these same samples. Here, we calculate 4, 2.6, 1.8, 1.4, and 1.1 for the A, F, G, K, and M stars, respectively. Again, the values need to be interpreted with caution because error estimation is difficult. To circumvent the difficulties in determining errors, we binned the excesses into intervals of 0.5 in excess ratio and used the K-S test to determine if the resulting distributions were likely to have been drawn from the identical parent distribution. For each stellar type, we tested the relevant distribution against the distribution for all the stars, excluding the contribution of the spectral type in question. The result was a set of probabilities of 0.03, 0.8, 0.3, 0.3, and 0.01 that the types A, F, G, K, and M, respectively, were drawn from the same parent distribution as the other types. (For this test, a claim of a significant difference requires a probability of 0.05 or less that the samples are from the same distribution. Values of 0.3 imply that the the G and K stars are 1σ different from their respective control samples.) From this suite of tests, we conclude that the incidence of excesses is different for old A stars and for M stars from that of the rest of our sample. We further deduce that there is a possibility of a difference appearing in the K stars from their lower average excess ratio. The distributions for F and G stars appear to be indistinguishable with our data. We employ this conclusion in the creation of an FG “supersample” (Section 6.4).

The higher excesses indicated for the old A stars could be an age effect, since the sample is by necessity significantly younger than the later types (which we selected in general to be > 1 Gyr in age). In fact, Gorlova et al. (2006) and Siegler et al. (2007) compare $24\mu\text{m}$ excesses from young A and solar-like stars and find that the incidence is quite similar at a given age. Age effects would presumably cause an apparent decrease of excess incidence with

later type among the F, G, and K stars because F stars will evolve off the main sequence quickly enough to bias our sample toward younger objects (Section 6.3).

In the end, this discussion may still be suffering from a relatively small number of K stars sampled. An ongoing *Spitzer* program (PID 30490) to survey nearby stars that were not observed in other programs — a sample that includes ~ 400 K stars — should help unravel these statistics. Nonetheless, given our result, it is unlikely that future surveys will find a strong trend among F, G, and K stars of comparable ages — a range of spectral types that spans more than a factor of 50 in stellar luminosity. This behavior is counter to our expectations and is a challenge to models of debris disk evolution.

6.3. Effects of age

The lack of strong dependence on spectral type lets us combine data on various types to study the evolution with stellar age. Figure 12 shows individual R24 and χ_{70} determinations for the stars in our FGK sample whose ages are known, as a function of system age. There is no correlation apparent for these individual sources, so we look to binned data in a larger combined sample for evidence of trends.

We once again take the union of the data presented here and that presented in Beichman et al. (2006b), but this time we include only spectral types F0–K5 from the Beichman et al. (2006b) sample (that is, we exclude the latest K stars). This is because the data we present in this paper covers the range F0–K5, and we want the best match to our combined sample. There are 10 stars in the F0–K5 TPF/SIM subsample that have no known ages, and 10 additional stars with ages less than 1 billion years. Of these 20, 2 systems have excesses (10%). Since this excess ratio is not significantly different from that of the overall FGK sample, and since the PID 30211 F stars sample is controlled for age but the PID 41 sample is not specifically controlled for age, we make no attempt to correct the larger sample for age.

Figure 13 shows excess rate as a function of age for this combined sample. To zeroth order, there is no trend as a function of age: a constant excess rate of $\sim 20\%$ adequately fits the data, being consistent at 1σ with the 10 Gyr data point and at 1.5σ with the 8 Gyr data point. Furthermore, the 10 Gyr bin has only 7 targets in it, and the 8 Gyr bin has only 33 targets in it (still a relatively small number).

On the other hand, we note that the data shown in Figure 13 is suggestive of an excess rate that decreases with time through at least 8 Gyr. In this scenario, the 10 Gyr bin would be highly anomalous, although we note that this bin is clearly affected by small number statistics (2 excesses out of 7 stars). In other words, there may be a real trend and a real

evolution of planetary systems and debris disks even on the billion-year timescale. However, this may again be a manifestation of the (potential) observational bias shown in Figure 8, as follows.

The fraction of stars in a given age bin that are K stars increases for the later age bins. If K stars truly have fewer excesses (or fewer detectable excesses, according to observational biases) than other spectral types, Figures 13 and 14 might indeed be showing a real decrease with increasing age, but caused not by a long-timescale evolution of planetary systems but by the increasing dominance of excess-deficient K stars at the oldest ages. The data present in our larger sample cannot distinguish between the competing possibilities of K stars preferentially lacking (detectable) disks, or of old stars increasingly lacking disks. It also remains to be seen whether the high excess rate for the oldest bin in Figure 13 is anything more than a small number statistics anomaly.

The overall high rate of excess incidence in our samples (17%) indicates that the 400 Myr decay timescale that drives the evolution of A star debris disks (Su et al. 2006) cannot drive the evolution of debris disks in our >1 Gyr Sun-like sample. Instead, Sun-like stars appear to have a relatively constant incidence of 15%–20% that is not strongly dependent on age, but may be weakly dependent on age through a very long timescale decrease.

6.4. Debris disks around Sun-like stars

Because there is no difference in excess rate between F and G stars, we can combine our sample of F0–G9 stars into a single population of “Sun-like” stars. To this sample of 169 stars we add the 56 F and G stars from Beichman et al. (2006b) to create an even larger sample of 225 Sun-like stars (213 stars at 24 microns). We refer to this merged sample of 213 and 225 stars as the “Sun-like supersample.” The excess rates for this supersample are $4.2^{+2.0}_{-1.1}\%$ at 24 microns and $16.4^{+2.8}_{-2.9}\%$ at 70 microns (Table 4). With this large supersample, we can now state the debris disk incidence rate for Sun-like stars with quite good confidence (small error bars).

6.5. Implications for planetary system formation

The majority of the debris disk systems that we present here have excesses at 70 microns only, suggesting temperatures $\lesssim 100$ K and therefore an inner edge to the disks. These dusty debris disks are likely produced by collisions within a swarm of planetesimals akin to the asteroid belt or Kuiper Belt in our Solar System. We interpret the cool temperatures we

derive for the dust in these disks as evidence of inner disk holes where the surface density of dust is much smaller than in the planetesimal ring, and potentially zero. This architecture is strongly reminiscent of our Solar System, where planets sculpt the edges of the planetesimal and dust belts. It may be that many of the systems we discuss here similarly have planets sculpting their dust distributions. In several cases, the known planets may indeed be the ones sculpting the inner edges of the disks (Tables 5 and 6). Additionally, Lawler et al. (in prep.) have found, using IRS spectra, that the incidence of detectable levels of warm dust may be higher than the 4.2% we find here, indicating that dust in a region analogous to our Solar System’s asteroid belt may also be somewhat common.

Bryden et al. (2007) show that the properties of disks around planet-bearing stars are unlikely to be similar to the properties of disks around stars without known planets. Briefly, the detection rates between these two populations are similar, but the planet-bearing stars are generally farther away and in more confused regions of the sky. They conclude that disks around planet-bearing stars are dustier (i.e., more massive), and probably more common, than disks around stars without known planets. Additionally, Trilling et al. (2007) recently showed that the excess rate for binary A-F stars is 9% and 40% at 24 and 70 μm , respectively, significantly higher than our results for FGK stars and for Sun-like stars. We see in Figure 11 that these excess rates are relatively high, compared to the large sample of single stars we present here. Combining these two studies, we find strong evidence that the presence of additional massive bodies (whether stellar or planetary companions) in stellar systems appears to promote higher excess rates. This effect may simply be dynamical — more massive bodies means more stirring, more collisions, and more dust — but it is not clear that such a process could remain effective for billions of years. Further work is necessary to explain these results.

Figure 11 shows that the transition from the high excess rate around A stars to the more modest excess rate around Sun-like stars is gradual. This gradual decay is likely an age effect (consider the mean ages of the samples given in Figure 11). Our data show that excess rates for FGK stars decline slowly with stellar age, and it is not clear whether we are detecting a billion-year tail of debris disk evolution, a dependence on spectral type, and/or an observational bias.

Young (<1 Gyr) debris disks decay on 100–400 million year timescales (Rieke et al. 2005; Su et al. 2006; Gorlova et al. 2006; Siegler et al. 2007). The presence of excesses around 16% of Sun-like stars at billion year ages indicates that these old debris disks must be driven by a different evolutionary process than debris disks around those younger stars. One interpretation, using our Solar System as an analogy, is that the younger systems are still active in a Late Heavy Bombardment kind of dynamical upheaval. After a billion years, such

large scale processes likely have ceased in all but the most unusual systems. Debris disks are then produced from collisions within remaining planetesimal belts (e.g., our asteroid belt) that have been dynamically excited by the previous eon’s dynamical stirring. However, there is no trend of fractional luminosity with age (Figure 14), although there is a lack of high fractional luminosity disks at old ages.

The presence of a debris disk indicates that planetary system formation progressed at least to the planetesimal stage in a given system. There is no apparent dependence on spectral type across Sun-like stars for fractional luminosity (i.e., dust mass), dust distance, or even excess rate. This indicates that the processes that give rise to debris disk — planetesimal formation, dynamical stirring that produces collisions — must equally be insensitive to stellar parameters (temperature, mass, luminosity). This may argue that planetary system formation is quite robust — able to occur in many different conditions. While none of the debris disks we observed are very similar to our own Solar System, there can be no question that the process of planetary system formation is quite common.

7. Summary

We observed nearly 200 FGK stars at 24 and 70 microns with the *Spitzer* Space Telescope to search for debris disks around nearby stars like the Sun. We identify excess emission, including a number of cases where the observed flux is more than 10 times brighter than the photospheric flux. We combine our data with results from several other sources to create a sample of more than 350 AFGKM stars. The incidence of debris disks in a large sample of Sun-like stars is $4.2^{+2.0}_{-1.1}\%$ at 24 microns (213 stars) and $16.4^{+2.8}_{-2.9}\%$ at 70 microns (225 stars). We find that the excess rates for A, F, G, and K stars are essentially indistinguishable, but with a suggestion of decreasing excess rate toward the later spectral types; this may be an age effect. The lack of strong trend among FGK stars of comparable ages is surprising, given the factor of 50 change in stellar luminosity across this spectral range. We also find that any decline in debris disk activity over the 1–10 Gyr time frame examined is very slow. This result contrasts with the more rapid decay found previously for stars 0.01–1 Gyr. This contrast suggests that the behavior at younger ages is dominated by events analogous to our Solar System’s Late Heavy Bombardment. How debris disks are maintained for the ensuing billions of years remains an outstanding question.

We thank suggestions from an anonymous referee that helped us clarify our results. This research has made use of NASA’s Astrophysics Data System (ADS abstract server); the SIMBAD databased, operated at CDS, Strasbourg, France; and of data products from

the Two Micron All Sky Survey, which is a joint project of the University of Massachusetts and the Infrared Processing and Analysis Center/California Institute of Technology, funded by the National Aeronautics and Space Administration and the National Science Foundation. This work is based in part on observations made with the *Spitzer* Space Telescope, which is operated by the Jet Propulsion Laboratory, California Institute of Technology under NASA contract 1407. Support for this work was provided by NASA through Contract Number 1255094 issued by JPL/Caltech.

Facilities: Spitzer (MIPS).

REFERENCES

- Alonso, A., Arribas, S., & Martinez-Roger, C. 1994, *A&AS*, 107, 365
- Alonso, A. et al. 1998, *A&AS*, 131, 209
- Aumann, H. H. 1985, *PASP*, 97, 885
- Aumann, H. H. et al. 1984, *ApJ*, 278, 23
- Backman, D. E. & Paresce, F. 1993, in *Protostars and Planets III*, eds. E. H. Levy & J. I. Lunine (Tucson: University of Arizona Press), 1253
- Barnes, S. 2007, *ApJ*, in press
- Beichman, C. A. et al. 2005a, *ApJ*, 622, 1160
- Beichman, C. A. et al. 2005b, *ApJ*, 626, 1061
- Beichman, C. A. et al. 2006a, *ApJ*, 639, 1166
- Beichman, C. A. et al. 2006b, *ApJ*, 652, 1674
- Bessell, M. S., Castelli, F., & Plez, B. 1998, *A&A*, 333, 231
- Bouchet, P., Schmider, F. X., & Manfroid, J. 1991, *A&AS*, 91, 409
- Bryden, G. et al. 2006, *ApJ*, 636, 1098
- Bryden, G. et al. 2007, *ApJ*, submitted
- Burgasser, A. J., Kirkpatrick, J. D., Reid, I. N., Brown, M. E., Miskey, C. L., & Gizis, J. E. 2003, *ApJ*, 586, 512

- Butler, R. P. et al. 2006, *ApJ*, 646, 505
- Carpenter, J. M. 2001, *AJ*, 121, 2851
- Carney, B. & Aaronson, M. 1979, *AJ*, 84, 867
- Cayrel de Strobel, G., Soubiran, C., & Ralite, N. 2001, *A&A*, 373, 159
- Chen, C. H. et al. 2006, *ApJS*, 166, 351
- Decin, G., Dominik, C., Malfait, K., Mayor, M., & Waelkens, C. 2000, *A&A*, 357, 533
- Decin, G., Dominik, C., Waters, L. B. F. M., & Waelkens, C. 2003, *ApJ*, 598, 626
- Drilling, J. S. & Landolt, A. U. 2000, in *Allen’s Astrophysical Quantities (Fourth Edition)*, ed. A. N. Cox (New York: Springer-Verlag), 381
- Engelbracht, C. W. et al. 2007a, *PASP*, in press (arXiv 0704.2195)
- Favata, F., Barbera, M., Micela, G., & Sciortino, S. 1993, *A&A*, 277, 428
- Fischer, D. A. & Valenti, J. 2005, *ApJ*, 622, 1102
- Gautier, T. N. et al. 2007, *ApJ*, in press
- Glass, I. 1974, *MNSSA*, 33, 53
- Glass, I. 1975, *MNRAS*, 171, 19
- Gonzalaz, G., Laws, C., Tyagi, S., & Reddy, B. E. 2001, *AJ*, 121, 432
- Gordon, K. D. et al. 2005, *PASP*, 117, 503
- Gordon, K. D. et al. 2007, *PASP*, in press (arXiv 0704.2196)
- Gorlova, N., Rieke, G. H., Muzerolle, J., Stauffer, J. R., Siegler, N. Young, E. T., & Stansberry, J. A. 2006, *ApJ*, 649, 1028
- Haas, M. & Leinert, Ch. 1990, *A&A*, 230, 87
- Habing, H. J. et al. 2001, *A&A*, 365, 545
- Hatzes, A. P. et al. 2000, *ApJ*, 544, L145
- Haywood, M. 2001, *MNRAS*, 325, 1365
- Johnson, H. L., Iriarte, B., Mitchell, R. I., & Wisniewski, W. Z. 1966, *Comm LPL*, 4, 99

- Johnson, H. L. et al. 1968, *ApJ*, 152, 465
- Jourdain de Muizon, M. et al. 1999, *A&A*, 350, 875
- Jura, M. et al. 2004, *ApJS*, 154, 453
- Lee, M. H., Butler, R. P., Fischer, D. A., Marcy, G. W., & Vogt, S. S. 2006, *ApJ*, 641, 1178
- Lisse, C. M., Beichman, C. A., Bryden, G., & Wyatt, M. C. 2007, *ApJ*, 658, 584
- Lovis, C. et al. 2006, *Nature*, 441, 305
- Marsakov, V. A. & Shevelev, Y. G. 1995, *Bulletin d'Information du Centre de Donnees Stellaires*, 47, 13
- Mayor, M., Udry, S., Naef, D., Pepe, F., Queloz, D., Santos, N. C., & Burnet, M. 2004, *A&A*, 415, 391
- McGregor, P. 1994, *PASP*, 106, 508
- Moór, A., Ábrahám, P., Derekas, A., Kiss, C., Kiss, L. L., Apai, D., Grady, C., & Henning, T. 2006, *ApJ*, 644, 525
- Mould, J. & Hyland, A. R. 1976, *ApJ*, 208, 399
- Nordstrom, B. et al. 2004, *A&A*, 419, 989
- Perryman, M. A. C. et al. 1997, 323, L49
- Persson, S. E., Aaronson, M., & Frogel, J. A. 1977, *AJ*, 82, 729
- Rieke, G. H. et al. 2004, *ApJS*, 154, 25
- Rieke, G. H. et al. 2005, *ApJ*, 620, 1010
- Santos, N. C., Israelian, G., & Mayor, M. 2001, *A&A*, 373, 1019
- Siegler, N., Muzerolle, J., Young, E. T., Rieke, G. H., Mamajek, E. E., Trilling, D. E., Gorlova, N., & Su, K. Y. L. 2007, *ApJ*, 654, 580
- Skrutskie, M. F. et al. 2006, *AJ*, 131, 1163
- Sousa, S. G., Santos, N. C., Israelian, G., Mayor, M., & Monteiro, M. J. P. F. G. 2006, *A&A*, 458, 873

- Spangler, C., Sargent, A. I., Silverstone, M. D., Becklin, E. E., & Zuckerman, B. 2001, *ApJ*, 555, 932
- Stapelfeldt, K. R. et al. 2006, *BAAS*, 209, #13.05
- Stencel, R. E. & Backman, D. E. 1991, *ApJS*, 75, 905
- Su, K. Y. L. et al. 2006, *ApJ*, 653, 675
- Teplitz, V. L., Stern, S. A., Anderson, J. D., Rosenbaum, D., Scalise, R. J., & Wentzler, P. 1999, *ApJ*, 516, 425
- Tokunaga, A. T. 2000, in *Allen’s Astrophysical Quantities (Fourth Edition)*, ed. A. N. Cox (New York: Springer-Verlag), 143
- Trilling, D. E. et al. 2007, *ApJ*, 658, 1289
- Udry, S., Fischer, D., & Queloz, D. 2007, in *Protostars and Planets V*, eds. B. Reipurth et al. (Tucson: University of Arizona Press), 685
- Valenti, J. & Fischer, D. A. 2005, *ApJS*, 159, 141
- Veeder, G., 1974, *AJ*, 79, 1056
- Vogt, S. S., Butler, R. P., Marcy, G. W., Fischer, D. A., Henry, G. W., Laughlin, G., Wright, J. T., & Johnson, J. A. 2005, *ApJ*, 632, 638
- Werner, M. W. et al. 2004, *ApJS*, 154, 1

Table 1. Target information

Name	Spec. type	V (mag)	d (pc)	Age (Gyr)	[M/H]	Ref.
63	F5	7.15	50.48	2.9	-0.08	M
142 ^a	G1IV	5.70	25.64	2.88	0.04	Ca
166	K0V	6.13	13.70	5.01	-0.30	Ca
693	F5V	4.89	18.89	5.16	-0.34	Ca
1237 ^a	G6V	6.7	17.62	2.75	0.10	Ca
1539	F5	7.03	46.32	2.9	0.03	M
1581	F9V	4.20	8.59	3.02	-0.10	Ca
3126	F2	6.92	41.51	3.5	-0.22	M
3296	F5	6.61	47.19	2.5	0.01	M
3302	F6V	5.52	36.22	7.76	-0.02	M
3651 ^a	K0V	5.80	11.11	5.89	0.26	Hy
3795	G3V	6.14	28.56	7.24	-0.73	Ca
3823	G1V	5.88	25.47	5.50	-0.35	Ca
3861	F5	6.53	33.34	3.4	0.03	M
4307	G2V	6.15	31.86	7.76	-0.36	Ca
4628	K2V	5.75	7.46	8.13	-0.29	Ca
7570	F8V	4.96	15.05	4.33	0.08	Ca
8070	F2	6.66	48.69	2.5	-0.20	M
8574 ^a	F8	7.8	44.15	7.24	-0.23	M
9826 ^a	F8V	4.09	13.47	6.31	-0.03	Ca
10476	K1V	5.20	7.47	4.57	-0.20	Ca
10647 ^a	F9V	5.52	17.35	6.3	-0.11	M
10697 ^a	G5IV	6.29	32.56	7.41	0.10	Ca
10800	G2V	5.89	27.13	7.37	0.03	M
13445 ^a	K1V	6.17	10.95	5.56	-0.21	Ca
13555	F5V	5.24	30.13	2.74	-0.18	Ca
14412	G5V	6.34	12.42	3.31	-0.53	Ca
14802	G2V	5.19	21.93	6.76	0.00	Ca
15335	G0V	5.91	30.79	7.76	-0.22	Ca
15798	F5V	4.75	25.82	3.16	-0.30	Ca

Table 1—Continued

Name	Spec. type	V (mag)	d (pc)	Age (Gyr)	[M/H]	Ref.
16160	K3V	5.82	7.21	5.4 ^b	-0.04	Hy
17051 ^a	G0V	5.40	17.24	2.43	-0.04	Ca
17925	K1V	6.00	10.38	0.19	-0.15	Ca
19373	G0V	4.05	10.53	5.89	0.03	Ca
19994 ^a	F8V	5.06	22.38	3.55	0.09	Ca
20367 ^a	G0	6.41	27.13	...	-0.01	M
20630	G5Ve	4.83	9.16	0.29	-0.01	Ca
20766	G2V	5.54	12.12	5.20	-0.20	Ca
20807	G1V	5.24	12.08	7.88	-0.20	Ca
22484	F8V	4.28	16.84	8.32	0.00	Ca
23079 ^a	G0V	7.1	34.6	7.89	-0.12	M
23596 ^a	F8	7.24	51.98	...	0.04	M
26923	G0IV	6.33	21.19	...	0.17	Ca
27442 ^a	K2Iva	4.44	18.23	6.6	0.22	Ca
28185 ^a	G5	7.81	39.56	3.45	0.25	So
30495	G1V	5.50	13.32	1.32	0.10	Ca
30652	F6V	3.19	8.03	1.55	0.01	M
33262	F7V	4.72	11.65	3.52	-0.23	Ca
33564 ^a	F6V	5.10	20.98	3.48	-0.11	M
33636 ^a	G0	7.06	28.69	3.24	-0.14	M
34411	G1.5IV-V	4.70	12.65	6.76	-0.08	Ca
34721	G0V	5.96	24.93	6.17	-0.25	Ca
35296	F8Ve	5.00	14.66	3.76	0.00	Ca
37394	K1Ve	6.23	12.09	0.49	-0.20	Ca
39091 ^a	G1V	5.67	18.21	5.609	0.04	M
40979 ^a	F8	6.75	148.37	...	-0.03	M
43162	G5V	6.37	16.69	0.37	-0.16	Hy
43834	G6V	5.09	10.15	7.61	0.00	Ca
50554 ^a	F8V	6.86	31.03	4.68	-0.12	M
50692	G0V	5.76	17.27	4.47	-0.11	M

Table 1—Continued

Name	Spec. type	V (mag)	d (pc)	Age (Gyr)	[M/H]	Ref.
52265 ^a	G0	6.30	28.07	6.03	0.21	Ca
52711	G4V	5.93	19.09	4.77	-0.16	Ca
55575	G0V	5.55	16.86	4.57	-0.28	Ca
57703	F2	6.78	44.09	2.3	-0.07	M
58855	F6V	5.37	19.90	3.6	-0.31	Ca
60912	F5	6.91	46.43	2.9	-0.04	M
62613	G8V	6.56	17.04	3.09	-0.20	Hy
63333	F5	7.11	43.07	5.5	-0.39	Ca
68456	F5V	4.76	21.39	2.43	-0.36	Ca
69830 ^a	K0V	5.95	12.58	4.68	-0.03	Ca
69897	F6V	5.10	15.67	3.55	-0.26	Ca
70843	F5	7.04	46.53	1.6	-0.01	M
71148	G5V	6.30	21.79	4.68	0.07	M
71640	F5	7.41	44.92	5.7	-0.09	M
72905	G1.5V	5.65	13.85	0.42	-0.08	Ca
75616	F5	6.99	35.61	4.8	-0.17	M
75732 ^a	G8V	5.95	12.53	6.46	0.40	Ca
76151	G3V	6.00	11.29	1.84	-0.02	Ca
77967	F0	6.60	40.7	3.5	-0.37	M
79392	F2	6.760	50.53	1.8	-0.24	M
80218	F5	6.629	39.20	6.4	-0.28	Ca
82943 ^a	G0	6.54	27.46	4.07	0.32	Ca
83451	F5	7.14	48.47	3.8	-0.14	M
83525	F5	6.91	48.38	5.3	-0.06	M
84117	G0V	4.94	14.88	4.24	-0.14	M
84737	G0.5Va	5.10	18.43	11.75	0.04	Ca
86147	F5	6.72	45.11	2.8	0.03	M
88230	K2Ve	6.61	4.69	4.68	-0.93	Ce
88984	F5	7.30	51.39	4.4	-0.29	M
90839	F8V	4.83	12.82	3.39	-0.18	Ca

Table 1—Continued

Name	Spec. type	V (mag)	d (pc)	Age (Gyr)	[M/H]	Ref.
93081	F5	7.11	51.36	3.5	-0.23	M
94388	F6V	5.24	31.34	3.16	0.07	Ca
95128 ^a	G0V	5.10	13.91	6.03	0.01	Ca
99126	F5	6.96	47.37	5.7	-0.16	M
100067	F5	7.30	40.77	5.4	-0.34	M
101259	G6/8V	6.42	64.72	10.96	-0.60	VF
101501	G8Ve	5.32	9.54	1.12	0.03	Ca
102438	G5V	6.48	17.77	...	-0.36	Hy
102870	F9V	3.61	10.90	4.47	0.20	Ca
103773	F5	6.87	49.95	2.4	0.06	M
104731	F6V	5.15	24.20	1.83	-0.21	Ca
104985 ^a	G9III	5.80	102.04	...	-0.18	M
105912	F5	6.95	50.25	1.8	-0.04	M
109756	F5	6.98	46.55	3.4	-0.22	M
110897	G0V	6.00	17.37	9.7	-0.59	Ca
111395	G7V	6.31	17.17	1.23	0.18	Hy
111545	F5	6.9	48.45	1.7	-0.02	M
112164	G1V	5.89	39.73	3.43	0.24	Ca
114613	G3V	4.85	20.48	5.27	0.16	VF
114710	F9.5V	4.26	9.15	2.29	0.06	Ca
114729 ^a	G3V	6.69	35.00	6.76	-0.26	FV
114783 ^a	K0V	7.57	20.43	4.37	-0.11	Hy
115383	G0V	5.22	17.95	0.40	0.04	Ca
115617	G5V	4.74	8.53	6.31	-0.03	Ca
117043	G6	6.50	21.34	...	0.22	Hy
117176 ^a	G5V	5.00	18.11	5.37	-0.09	Ca
118972	K1	6.93	15.60	...	-0.03	Hy
120005	F5	6.50	44.92	2.9	0.05	M
120136 ^a	F7V	4.50	13.51	1.91	0.30	Ca
120690	G5V	6.45	19.92	2.24	-0.11	Ca

Table 1—Continued

Name	Spec. type	V (mag)	d (pc)	Age (Gyr)	[M/H]	Ref.
122862	G2.5IV	6.02	28.68	6.11	-0.11	M
123691	F2	6.80	50.89	1.5	-0.09	M
126660	F7V	4.10	14.57	2.76	-0.05	Ca
127334	G5V	6.40	23.57	6.92	0.05	Ca
128311 ^a	K0	7.51	16.57	...	0.08	Hy
130460	F5	7.23	48.31	3.5	-0.03	M
130948	G2V	5.88	17.94	0.87	0.20	Ca
133002	F9V	5.64	43.33	2.459
134083	F5V	4.93	19.72	1.73	0.00	Ca
134987 ^a	G5V	6.45	25.65	7.76	0.36	Ca
136064	F8V	5.10	25.31	4.64	-0.10	Ca
136118 ^a	F8	6.94	52.27	...	-0.15	M
141128	F5	7.01	51.02	3	-0.24	M
142373	F9V	4.62	15.85	8.13	-0.40	Ca
142860	F6IV	3.85	11.12	2.88	-0.13	Ca
143105	F5	6.76	46.08	3.3	-0.10	M
143761 ^a	G0V	5.40	17.43	7.41	-0.26	Ca
145675 ^a	K0V	6.67	18.15	6.92	0.50	Ca
146233	G1V	5.50	15.36	4.57	0.05	Ca
149661	K2V	5.76	9.78	1.17	0.00	Hy
152391	G8V	6.64	16.94	0.58	-0.18	Hy
154088	G8IV-V	6.59	18.08	5.89	0.30	Hy
157214	G2V	5.40	13.57	6.46	-0.41	Ca
160691 ^a	G3IV-V	5.15	15.28	6.67	0.16	Ca
166620	K2V	6.37	11.10	5.01	0.07	Hy
168151	F5V	5.03	23.50	2.53	-0.17	Ca
168443 ^a	G5V	6.92	37.88	8.51	0.10	Go
169830 ^a	F8	5.91	36.32	7.24	0.13	Ca
171886	F5	7.18	49.65	3.7	-0.33	M
173667	F6V	4.20	19.09	3.39	-0.01	Ca

Table 1—Continued

Name	Spec. type	V (mag)	d (pc)	Age (Gyr)	[M/H]	Ref.
176441	F5	7.08	44.72	3.7	-0.27	M
177830 ^a	K0	7.18	59.03	8.5	0.36	Go
181321	G5V	6.49	20.86	0.5
181655	G8V	6.31	25.23	4.57	0.02	VF
185144	K0V	4.70	5.61	3.24	-0.14	Hy
186408	G1.5V	5.96	21.62	10.4	0.08	Ca
186427 ^a	G3V	6.20	21.41	7.41	0.08	Ca
188376	G5V:	4.70	23.79	4.47	-0.13	Ca
189567	G2V	6.07	17.71	...	-0.30	Ca
190007	K4V	7.48	13.11	1.5 ^b
190248	G7IV	3.56	6.11	...	0.32	Ca
191408	K3V	5.31	6.05	7.88	-0.58	Ca
193664	G3V	5.93	17.57	4.7	-0.18	M
196050 ^a	G3V	7.6	46.93	...	0.23	FV
196378	F8V	5.12	24.20	6.02	-0.30	Ca
196761	G8V	6.37	14.65	4.27	-0.60	Hy
197692	F5V	4.15	14.67	1.94	0.04	Ca
200433	F5	6.92	48.36	1.4	-0.09	M
202884	F5	7.27	42.05	5.2	-0.29	M
203608	F8V	4.22	9.22	10.196	-0.64	Ca
206860	G0V	6.00	18.39	5.00	-0.20	Ca
207129	G0V	5.58	15.64	5.76	-0.15	Ca
209100	K4.5V	4.69	3.63	1.38	0.04	Ca
210277 ^a	G0V	6.63	21.29	6.76	0.22	Ca
210302	F6V	4.92	18.74	5.37	0.06	Ca
210918	G5V	6.26	22.13	3.85	-0.18	Ca
212330	G3IV	5.31	20.49	7.94	0.00	Ca
212695	F5	6.95	51.10	2.3	-0.05	M
213240 ^a	G0V	6.80	40.75	2.77	0.04	M
216345	G8III	10.21	100

Table 1—Continued

Name	Spec. type	V (mag)	d (pc)	Age (Gyr)	[M/H]	Ref.
216437 ^a	G2.5IV	6.06	26.52	7.15	0.10	Ca
216803	K4V	6.48	7.64	0.2 ^b	0.07	Sa
217014 ^a	G4V	5.49	17.12	7.41	0.05	Ca
217813	G5	6.66	24.27	0.71	-0.07	M
219134	K3V	5.56	6.53	...	0.20	Hy
219983	F2	6.67	47.71	4.7	-0.27	M
220182	K1	7.36	21.92	0.26	0.01	Hy
221420	G2V	5.82	31.76	5.52	0.37	So
222143	G5	6.58	23.12	...	0.08	Hy
222368	F7V	4.13	13.79	3.93	-0.18	Ca
222404 ^a	K1IV	3.23	13.79	...	-0.05	Ca
222582 ^a	G3V	7.70	41.95	6.63	0.02	Go
225239	G2V	6.10	36.79	...	-0.50	Ca

^aStar with known planet(s).

^bAge from Barnes (2007).

Note. — Spectral types and V magnitudes are from B06 and from SIMBAD and Hipparcos. Ages are from B06 and from Nordstrom et al. (2004) except as indicated. To date, Barnes (2007) has derived ages for $\sim 15\%$ of the stars in this sample, and in general the agreement with our compiled literature values is good. When the number examined becomes a significant fraction of the total sample, we will re-examine excesses as a function of age using the new, systematic age definitions (future work). Distances are from Hipparcos (Perryman et al. 1997). A number of stars have no good ages, and a handful have no good metallicities. Metallicities are

from the indicated references: (Ca) Cayrel de Strobel et al. (2001); (FV) Fischer & Valenti (2005); (Go) Gonzelaz et al. (2001); (Hy) Haywood (2001); (M) Marsakov & Shevelev (1995); (Sa) Santos et al. (2001); (So) Sousa et al. (2006); (VF) Valenti & Fischer (2005).

Table 2. Observing log

Name	Int. time 24 μm (sec)	Int. time 70 μm (sec)	AORKey ^a	PID
63	48	355	17346304	30211
142	0	1090	12715008	41
142	48	355	4082176	41
166	48	440	4030720	41
693	48	440	4030976	41
1237	48	1300	4060672	41
1539	48	231	17343232	30211
1581	48	126	4031232	41
3126	48	231	17337600	30211
3296	48	132	17340672	30211
3302	48	440	4031488	41
3651	48	231	4031744	41
3795	48	650	4032000	41
3823	48	440	4032256	41
3861	48	107	17335552	30211
4307	48	650	4032512	41
4628	48	126	4032768	41
7570	48	231	4033024	41
8070	48	231	17341696	30211
8574	0	1007	4005376	41
8574	92	2181	8775936	41
9826	48	231	4033280	41
10476	48	126	4033536	41
10647	136	336	7865856	717
10697	48	881	4033792	41
10800	48	440	4034048	41
13445	48	126	4034304	41
13555	48	440	4034560	41
14412	48	881	4034816	41

Table 2—Continued

Name	Int. time 24 μm (sec)	Int. time 70 μm (sec)	AORKey ^a	PID
14802	48	126	4035072	41
15335	48	650	4035328	41
15798	48	440	4035584	41
16160	48	231	4035840	41
17051	48	355	4036096	41
17925	48	126	4036352	41
19373	48	126	4036608	41
19994	48	440	4080640	41
20367	48	1300	12711936	41
20630	48	126	4036864	41
20766	48	231	4037120	41
20807	48	440	4037376	41
22484	48	231	4006400	41
23079	48	2181	4080384	41
23596	48	2181	12711168	41
26923	48	1300	4060928	41
27442	48	126	4081152	41
28185	136	2181	4005632	41
30495	48	231	4037632	41
30652	48	231	4037888	41
33262	48	126	4038144	41
33564	48	231	4038400	41
33636	0	1300	4059136	41
33636	48	2181	8777728	41
34411	48	126	4038656	41
34721	48	650	4038912	41
35296	48	231	4061184	41
37394	48	126	4039168	41
39091	48	355	4039424	41

Table 2—Continued

Name	Int. time 24 μm (sec)	Int. time 70 μm (sec)	AORKey ^a	PID
40979	48	2181	12711680	41
43162	48	1007	4039680	41
43834	48	126	4039936	41
50554	0	1300	4080128	41
50554	48	2181	8775680	41
50692	48	440	4040192	41
52265	0	1090	12715776	41
52265	48	1090	4062976	41
52711	48	440	4040448	41
55575	48	355	4040704	41
57703	48	231	17338880	30211
58855	48	355	4040960	41
60912	48	231	17342976	30211
62613	48	1090	4041216	41
63333	48	231	17338112	30211
68456	48	231	4041472	41
69830	48	355	4041728	41
69897	48	231	4006144	41
70843	48	231	17344000	30211
71148	48	881	4041984	41
71640	48	355	17346560	30211
72905	48	355	4042240	41
75616	48	231	17336064	30211
75732	48	440	4042496	41
76151	48	545	4042752	41
77967	48	126	17336832	30211
79392	48	231	17342720	30211
80218	48	107	17336576	30211
82943	48	1636	4063232	41

Table 2—Continued

Name	Int. time 24 μm (sec)	Int. time 70 μm (sec)	AORKey ^a	PID
83451	48	231	17342464	30211
83525	48	231	17341952	30211
84117	48	126	4043008	41
84737	48	231	4043264	41
86147	48	132	17340416	30211
88230	48	231	4043776	41
88984	48	355	17347840	30211
90839	48	231	4006656	41
93081	48	355	17345024	30211
94388	48	440	4044032	41
95128	48	231	4044288	41
99126	48	231	17341440	30211
100067	48	355	17337088	30211
101259	48	1090	4044544	41
101501	48	231	4044800	41
102438	48	1090	4045056	41
102870	48	126	4045312	41
103773	48	231	17340928	30211
104731	48	440	4045824	41
104985	48	440	12712192	41
105912	48	355	17345280	30211
109756	48	231	17342208	30211
110897	48	755	4046080	41
111395	48	755	4046336	41
111545	48	355	17344768	30211
112164	48	440	4046592	41
114613	48	355	4046848	41
114710	48	126	4047104	41
114729	48	1510	4084480	41

Table 2—Continued

Name	Int. time 24 μm (sec)	Int. time 70 μm (sec)	AORKey ^a	PID
114783	48	2181	4055552	41
115383	48	231	4047360	41
115617	0	1321	12712960	41
115617	48	126	4047616	41
117043	48	1007	4047872	41
117176	0	440	12716800	41
117176	48	126	4048128	41
118972	48	440	4048384	41
120005	48	107	17339648	30211
120136	48	126	4048640	41
120690	48	1090	4048896	41
122862	48	545	4049152	41
123691	48	355	17344512	30211
126660	48	126	4006912	41
127334	48	1007	4049408	41
128311	0	1090	4083456	41
128311	48	2181	8776192	41
130460	48	355	17347584	30211
130948	48	440	4049664	41
133002	48	440	4049920	41
134083	48	231	4050176	41
134987	48	1090	4050432	41
136064	48	231	4050688	41
136118	92	2181	12712448	41
141128	48	355	17345792	30211
142373	48	126	4050944	41
142860	48	126	4051200	41
143105	48	132	17340160	30211
143761	48	355	4051456	41

Table 2—Continued

Name	Int. time 24 μm (sec)	Int. time 70 μm (sec)	AORKey ^a	PID
145675	48	1007	4051712	41
146233	48	231	4081664	41
149661	48	126	4051968	41
152391	48	1300	4061440	41
154088	48	1300	4061696	41
157214	48	231	4007168	41
160691	48	126	4061952	41
166620	48	231	4052224	41
168151	48	355	4052480	41
168443	48	126	4052736	41
169830	48	545	4063488	41
171886	48	355	17346048	30211
173667	48	126	4052992	41
176441	48	355	17339392	30211
177830	48	2181	4053248	41
181321	48	1300	4062208	41
181655	48	755	4053504	41
185144	48	126	4053760	41
186408	48	755	4054016	41
186427	48	755	4054016	41
188376	48	126	4054272	41
189567	48	545	4054528	41
190007	48	1007	4082432	41
190248	48	126	4054784	41
191408	48	126	4055040	41
193664	48	440	4055296	41
196050	48	2181	12711424	41
196378	48	231	4055808	41
196761	48	881	4056064	41

Table 2—Continued

Name	Int. time 24 μm (sec)	Int. time 70 μm (sec)	AORKey ^a	PID
197692	48	126	4056320	41
200433	48	231	17343744	30211
202884	48	355	17347328	30211
203608	48	126	4056576	41
206860	48	650	4056832	41
207129	48	126	4057088	41
209100	48	126	4057344	41
210277	48	1950	4057600	41
210302	48	231	4057856	41
210918	48	755	4058112	41
212330	48	231	4058368	41
212695	48	231	17343488	30211
213240	0	355	4080896	41
213240	48	2181	8776448	41
216345	48	881	12712704	41
216437	48	545	4083968	41
216803	48	440	4058624	41
217014	48	231	4058880	41
217813	48	1510	4062464	41
219134	48	231	4059392	41
219983	48	107	17339904	30211
220182	48	1007	4062720	41
221420	48	440	4059648	41
222143	48	1090	4059904	41
222368	48	231	4060160	41
222404	48	231	12710912	41
222582	92	2181	4005888	41
225239	48	650	4060416	41

^aFurther details of each observation, including pointing and time and date of observation, can be queried from the *Spitzer* Data Archive at the *Spitzer* Science Center using the specified AORKey.

Note. — HD 10647 was observed in PID 717, a MIPS in-orbit check-out (IOC) program.

Table 3. Photospheric predictions and photometry for all sources

Name	V (mag)	K (mag)	F24 (mJy)	P24 (mJy)	R24	F70 (mJy)	σ_{70} (mJy)	P70 (mJy)	χ_{70}
63	7.13	6.01	29	28	1.02	6	3	3	0.86
142	5.70	4.47	122	117	1.05	28	6	13	2.60
166	6.07	4.31	158	138	1.15	104	4	15	22.57
693	4.89	3.617 ^b	255	252	1.01	39	4	28	2.95
1237	6.59	4.86	82	83	1.00	11	2	9	0.89
1539	7.03	5.82	34	33	1.01	-0.1	3	4	-1.19
1581	4.23	2.77	546	558	0.98	84	6	60	4.06
3126	6.9	5.75	41	35	1.16	108	3	4	35.58
3296	6.72	5.59	42	41	1.02	24	3	5	6.81
3302	5.51	4.50	120	112	1.07	10	5	13	-0.63
3651	5.88	4.00	191	184	1.04	16	6	21	-0.92
3795	6.14	4.33	135	133	1.01	19	2	15	1.60
3823	5.89	4.49	114	115	0.99	14	4	13	0.22
3861	6.52	5.28	54	55	0.98	4	3	6	-0.54
4307	6.15	4.62	101	102	0.99	10	4	11	-0.28
4628	5.74	3.566 ^c	278	275	1.01	26	10	31	-0.44
7570 ^a	4.97	3.50 ^d	255	284	0.90	44	7	28	2.46
8070	6.65	5.61	39	40	0.97	2	3	4	-0.92
8574	7.12	5.78	34	35	0.98	3	2	4	-0.44
9826	4.10	2.86	527	513	1.03	55	5	58	-0.64
10476	5.24	3.24 ^e	360	371	0.97	53	8	40	1.70
10647	5.52	4.17 ^f	187	154	1.21	859	6	17	136.40
10697	6.27	4.60	100	105	0.95	1	5	11	-2.11
10800	5.88	4.41	124	125	1.00	14	3	14	-0.01
13445	6.12	4.13	163	164	0.99	5	7	18	-1.79
13555	5.23	4.12	167	160	1.05	19	5	18	0.26
14412	6.33	4.55	112	110	1.02	14	2	12	0.97
14802	5.19	3.68 ^d	259	242	1.07	36	6	28	1.15
15335	5.89	4.48	120	116	1.04	8	4	13	-1.21
15798	4.74	3.56 ^b	267	267	1.00	22	5	29	-1.49

Table 3—Continued

Name	V (mag)	K (mag)	F24 (mJy)	P24 (mJy)	R24	F70 (mJy)	σ_{70} (mJy)	P70 (mJy)	χ_{70}
16160	5.79	3.44 ^g	311	311	1.00	35	6	34	0.28
17051	5.40	4.14	167	159	1.05	22	3	18	1.34
17925	6.05	4.02 ^c	191	182	1.05	71	5	21	9.14
19373	4.05	2.65 ^c	626	626	1.00	57	7	69	-1.59
19994	5.07	...	241	43	4	26	4.25
20367	6.40	5.04	67	69	0.97	9	4	7	0.56
20630	4.84	3.24 ^h	355	366	0.97	42	7	39	0.43
20766	5.53	3.99 ^d	189	183	1.03	30	4	21	2.16
20807	5.24	3.77 ^d	233	223	1.05	46	4	26	5.44
22484	4.29	2.88 ^c	514	504	1.02	108	5	56	9.58
23079	7.12	5.71	37	37	0.98	5	1	4	0.95
23596	7.25	5.87	33	32	1.02	4	4	4	0.058
26923	6.32	4.90	76	78	0.97	7	3	8	-0.57
27442	4.44	1.93 ^j	1148	1248	0.92	136	5	126	1.82
28185	7.80	6.19	23	24	0.94	1	5	3	-0.31
30495	5.49	4.00	191	181	1.06	116	4	21	26.58
30652	3.19	2.05 ^g	1060	1071	0.99	118	5	116	0.38
33262	4.71	3.39 ^d	325	315	1.03	61	5	36	4.83
33564	5.08	3.91	185	194	0.95	25	5	20	1.00
33636	7.00	5.57	42	42	0.99	35	2	5	13.81
34411	4.69	3.24 ^c	363	363	1.00	40	10	40	0.05
34721	5.96	4.56	109	108	1.01	6	3	12	-1.81
35296	5.00	3.67 ^f	238	243	0.98	31	6	26	0.67
37394	6.21	4.27	139	143	0.97	30	6	15	2.42
39091	5.65	4.24	139	145	0.96	23	3	15	2.69
40979	6.74	5.45	47	47	1.00	14	6	5	1.50
43162	6.37	4.73	94	93	1.01	15	2	10	2.19
43834	5.08	3.40 ^d	309	316	0.98	44	11	34	0.95
50554	6.84	5.47	46	46	1.00	42	4	5	9.29
50692	5.74	4.29	136	138	0.99	12	11	15	-0.28

Table 3—Continued

Name	V (mag)	K (mag)	F24 (mJy)	P24 (mJy)	R24	F70 (mJy)	σ_{70} (mJy)	P70 (mJy)	χ_{70}
52265	6.29	4.95	74	75	0.98	38	5	8	5.63
52711	5.93	4.54	116	111	1.05	14	4	13	0.24
55575	5.54	4.12	166	162	1.02	30	4	18	2.91
57703	6.78	5.69	38	37	1.02	37	3	4	9.67
58855	5.35	4.18	153	152	1.01	14	3	17	-0.85
60912	6.89	5.81	35	34	1.03	3	3	4	-0.15
62613	6.55	4.86	83	83	1.00	11	3	9	0.53
63333	7.09	5.79	35	34	1.01	0.1	3	4	-1.19
68456	4.74	3.62 ^d	256	254	1.01	31	5	28	0.59
69830	5.95	4.17	232	158	1.47	26	3	17	2.82
69897	5.13	...	196	32	5	22	2.18
70843	7.06	5.869	32	32	1.01	9	7	4	0.78
71148	6.32	4.83	81	85	0.96	4	3	9	-2.11
71640	7.4	6.01	29	28	1.02	-0.7	2	3	-1.53
72905	5.63	4.17	164	154	1.06	42	3	18	7.71
75616	6.92	5.68	39	38	1.03	41	2	4	16.01
75732	5.96	4.02	172	181	0.95	21	4	19	0.46
76151	6.01	4.46	123	119	1.03	33	3	14	5.51
77967	6.61	5.42	48	48	1.00	2	4	5	-0.91
79392	6.75	5.76	37	35	1.05	3	3	4	-0.21
80218	6.61	5.31	53	54	0.98	6	8	6	0.04
82943	6.54	5.11	66	65	1.02	119	5	7	24.91
83451	7.12	5.76	35	35	1.01	1	3	4	-0.86
83525	6.9	5.65	38	39	0.99	8	3	4	1.42
84117	4.93	3.54 ^d	246	275	0.89	16	11	27	-0.9
84737	5.08	3.61	250	258	0.97	34	4	27	1.60
86147	6.7	5.58	42	41	1.00	-1	3	5	-1.78
88230	6.60	3.17 ^{c g k l}	428	396	1.08	39	4	47	-2.07
88984	7.3	6.06	27	27	1.00	-0.8	7	3	-0.54
90839	4.82	3.52 ^d	283	279	1.02	34	4	31	0.85

Table 3—Continued

Name	V (mag)	K (mag)	F24 (mJy)	P24 (mJy)	R24	F70 (mJy)	σ_{70} (mJy)	P70 (mJy)	χ_{70}
93081	7.09	5.91	31	31	1.00	9	3	3	2.02
94388	5.23	...	171	18	3	19	0.26
95128	5.03	...	268	32	4	29	0.67
99126	6.94	5.62	39	40	0.97	0.9	3	4	-1.24
100067	7.17	5.89	30	31	0.96	-6	2	3	-4.43
101259	6.40	4.48	148	118	1.25	21	3	13	3.33
101501	5.31	3.56 ^c	262	276	0.95	29	4	29	0.10
102438	6.48	4.80	85	87	0.98	12	4	9	0.82
102870	3.59	2.29 ^j	886	869	1.02	117	9	97	2.11
103773	6.73	5.62	40	40	1.00	1	3	4	-1.14
104731	5.15	4.09	171	165	1.04	5	7	19	-2.00
104985	5.78	...	351	37	4	39	-0.4
105912	6.95	5.91	47	31	1.53	32	2	3	11.97
109756	6.95	5.75	37	35	1.04	13	3	4	2.47
110897	5.95	4.47	115	117	0.98	56	4	13	11.56
111395	6.29	4.65	97	101	0.96	14	3	11	0.93
111545	6.99	5.90	31	31	1.00	4	2	3	0.29
112164	5.89	4.48	114	116	0.98	15	18	13	0.13
114613	4.85	3.23 ^j	366	370	0.99	55	5	40	2.63
114710	4.23	2.85 ^{c g k m}	507	517	0.98	47	6	56	-1.57
114729	6.68	5.14	62	64	0.98	10	3	7	1.17
114783	7.56	5.48	45	47	0.95	6	4	5	0.34
115383	5.19	...	216	19	6	24	-0.79
115617	4.74	3.06 ^d	449	433	1.04	195	8	49	18.31
117043	6.50	4.80	84	88	0.96	15	3	9	1.76
117176	4.97	3.20 ^c	372	380	0.98	72	4	41	7.33
118972	6.92	4.93	85	78	1.08	33	3	9	6.96
120005	6.51	5.23	57	57	0.99	8	3	6	0.59
120136	4.50	3.31 ^d	338	338	1.00	34	6	37	-0.56
120690	6.43	4.67	100	99	1.01	8	3	11	-0.94

Table 3—Continued

Name	V (mag)	K (mag)	F24 (mJy)	P24 (mJy)	R24	F70 (mJy)	σ_{70} (mJy)	P70 (mJy)	χ_{70}
122862	6.02	4.58	105	106	0.99	16	3	12	1.23
123691	6.8	5.86	33	32	1.03	7	2	4	1.59
126660	4.04	2.83 ^d	574	526	1.09	65	7	63	0.32
127334	6.36	4.73	88	92	0.95	10	2	10	-0.15
128311	7.48	5.14	60	64	0.93	21	3	7	4.29
130460	7.22	6.05	27	27	1.02	5	3	3	0.58
130948	5.86	4.46	117	119	0.98	9	3	13	-1.41
133002	5.63	3.92	201	193	1.04	23	2	22	0.59
134083	4.93	3.86 ^j	203	203	1.00	34	6	22	2.02
134987	6.47	4.88	76	81	0.94	4	8	8	-0.63
136064	5.15	...	207	21	5	23	-0.34
136118	6.93	5.60	39	41	0.94	3	3	4	-0.57
141128	7	5.93	30	30	1.00	8	3	3	1.73
142373	4.60	3.06 ^m	420	429	0.98	41	5	46	-0.96
142860	3.85	2.62 ^j	639	639	1.00	72	16	70	0.08
143105	6.76	5.52	44	44	1.00	7	3	5	0.84
143761	5.39	3.86	199	205	0.97	31	5	22	1.77
145675	6.61	4.71	92	95	0.96	11	2	10	0.03
146233	5.49	...	182	22	7	20	0.29
149661	5.77	3.85 ^l	211	213	0.99	31	6	23	1.33
152391	6.65	4.84	81	85	0.95	14	4	9	1.32
154088	6.59	4.76	87	91	0.96	2	7	10	-1.25
157214	5.38	3.82 ⁿ	216	214	1.01	25	4	24	0.24
160691	5.12	3.52 ^d	268	282	0.95	31	8	29	0.15
166620	6.38	4.23	146	149	0.98	7	4	16	-2.51
168151	4.99	...	208	23	3	23	0.07
168443	6.92	5.21	55	60	0.92	9	29	6	0.10
169830	5.90	4.69	98	95	1.03	10	7	11	-0.16
171886	7.16	5.98	29	29	0.99	0.8	2	3	-1.24
173667	4.19	3.02 ^d	442	439	1.01	69	7	49	2.93

Table 3—Continued

Name	V (mag)	K (mag)	F24 (mJy)	P24 (mJy)	R24	F70 (mJy)	σ_{70} (mJy)	P70 (mJy)	χ_{70}
176441	7.06	5.89	33	31	1.05	-5	3	4	-2.72
177830	7.18	4.81	88	87	1.01	6	3	10	-1.06
181321	6.48	4.93	80	78	1.03	4	6	9	-0.85
181655	6.29	4.68	92	98	0.94	7	3	10	-0.94
185144	4.67	2.74 ^c	567	591	0.96	71	5	62	1.79
186408	5.96	4.43	114	110	1.03	11	6	14	-0.61
186427	6.25	4.65	95	100	0.95	-1	5	10	-2.53
188376	4.70	2.95 ^d	515	477	1.08	51	11	57	-0.50
189567	6.07	4.51	110	113	0.98	19	3	12	1.90
190007	7.46	4.80	88	89	0.99	7	4	10	-0.66
190248	3.55	1.91 ^p	1262	1250	1.01	138	5	139	-0.08
191408	5.32	3.23 ^d	464	378	1.23	49	10	51	-0.19
193664	5.91	4.45	118	120	0.98	19	4	13	1.48
196050	7.50	6.03	26	28	0.95	2	3	3	-0.44
196378	5.11	...	229	32	3	25	1.97
196761	6.36	4.60	102	106	0.97	8	4	11	-0.85
197692	4.13	3.07 ^d	413	422	0.98	42	8	45	-0.50
200433	6.91	5.85	33	32	1.02	6	3	4	0.91
202884	7.27	6.03	28	28	1.03	8	2	3	2.03
203608	4.21	2.88 ^p	497	502	0.99	45	5	55	-1.88
206860	5.96	4.56	111	108	1.03	28	2	12	6.63
207129	5.57	...	164	289	11	18	24.6
209100	4.69	2.14 ^q	1039	1029	1.01	113	6	114	-0.23
210277	6.54	4.80	83	86	0.97	8	2	9	-0.55
210302	4.94	...	215	11	6	24	-2.1
210918	6.23	4.66	98	99	0.99	9	3	11	-0.65
212330	5.31	3.72 ^d	241	234	1.03	29	4	26	0.71
212695	6.94	5.82	33	33	0.99	38	3	4	11.59
213240	6.81	5.35	50	52	0.96	7	2	5	0.55
216345	8.08	7.97	5	5	0.98	3	4	1	0.65

Table 3—Continued

Name	V (mag)	K (mag)	F24 (mJy)	P24 (mJy)	R24	F70 (mJy)	σ_{70} (mJy)	P70 (mJy)	χ_{70}
216437	6.04	4.52	107	112	0.96	7	5	12	-0.98
216803	6.48	3.90 ^d	220	204	1.08	27	4	24	0.94
217014	5.45	3.91	189	197	0.96	27	4	21	1.36
217813	6.65	5.15	60	63	0.95	4	5	7	-0.52
219134	5.57	3.17 ^g	399	399	1.00	20	10	44	-2.51
219983	6.64	5.34	51	52	0.99	8	3	6	0.58
220182	7.36	5.47	46	48	0.96	5	3	5	0.05
221420	5.82	4.31	135	136	0.99	19	3	15	1.24
222143	6.58	5.08	67	68	0.99	7	2	7	-0.39
222368	4.13	2.9 ^f	517	493	1.05	60	7	57	0.40
222404	3.21	0.90 ^d	3551	3219	1.10	355	5	362	-1.4
222582	7.68	6.17	24	24	0.96	9	2	3	2.73
225239	6.10	4.44	126	121	1.04	10	4	14	-0.89

^aBeichman et al. (2006a) found that this system has a weak excess in the 30–34 micron region that is not evident in our 24 or 70 micron data.

^bMcGregor (1994)

^cJohnson et al. (1968)

^dDerived from B-I

^eAlonso et al. (1994)

^fDerived from B-V

^gGlass (1975)

^hBouchet et al. (1991)

^jJohnson et al. (1966)

^kVeeder (1974)

^lPersson et al. (1977)

^mAlonso et al. (1998)

ⁿCarney & Aaronson (1979)

^pGlass (1974)

^qMould & Hyland (1976)

^rHaas & Leinert (1990)

Note. — V magnitudes are from Hipparcos, with typical errors 0.01 mag (Perryman et al. 1997). K magnitudes are from 2MASS, with typical errors 0.02 mag (Skrutskie et al. 2006), except as indicated. All of these sources are strongly detected at 24 microns, with intrinsically large S/N. We calculate P70 as $F_{24}/9.10$, except for the six cases with 24 micron excesses and P24 (see text), where we calculate $P70=P24/9.10$. For HD 207129, a seventh star with 24 micron excess, we identify the excess through Kurucz fitting; see text. The implied excess for HD 191408 is spurious (see text). There are 12 stars for which K band data is not available, and therefore no P24 or R24 determinations. However, even for these stars, we can still find P70 as $F_{24}/9.10$, and measure χ_{70} . For these twelve stars, χ_{70} is actually a lower limit, since there could be small 24 micron excesses that we cannot measure.

Table 4. Summary of excess rates

Sample	24 micron Number	24 micron excess rate (%)	70 micron Number	70 micron excess rate (%)
A	30	7 (+3/-3)	27	26 (+10/-7)
FGK sample	184	3.8 (+1.7/-1.2)	196	16.3 (+2.9/-2.8)
FGK sample, planets	45	6.7 (+5.8/-2.1)	48	20.8 (+7.0/-4.6)
FGK sample, no planets	139	2.9 (+2.2/-0.8)	148	14.9 (+3.4/-2.5)
All F	110	7.3 (+3.3/-1.2)	117	17.9 (+4.1/-3.0)
All G	103	1.0 (+2.2/-1.0)	108	14.8 (+4.0/-2.8)
All K	51	5.9 (+5.2/-1.8)	51	13.7 (+6.2/-3.5)
M	62	0.0 (+2.9)	13	0.0 (+12)
Sun-like supersample (FG)	213	4.2 (+2.0/-1.1)	225	16.4 (+2.8/-2.9)

Note. — The A stars sample includes stars with ages ≥ 600 Myr from Su et al. (2006). The FGK sample is all data presented in this paper, from PIDs 41 and 30211, plus the three additional stars listed in Section 5.1. The “All F/G/K” samples are produced by combining data presented in this paper with data from Beichman et al. (2006b), for the given spectral types. The M stars results are taken directly from Gautier et al. (2007). The Sun-like supersample is defined in Section 6.4 as all F and all G stars from this paper and from Beichman et al. (2006b), combined. In all of these samples, all stars that have excesses at 24 microns also have excesses at 70 microns (except some of the A stars, where only upper limits are available at 70 microns for some sources). In all cases in this paper, we cite binomial errors that include 68% of the probability (equivalent to the 1σ range for gaussian errors), as defined in Burgasser et al. (2003).

Table 5. Color temperature for excesses detected at both bands

Name	F24 _{excess} (mJy)	F70 _{excess} (mJy)	T _{color} (K)	R _{dust} (AU)	f _d ×10 ⁻⁵
166	20	89	87	9.1	5.9
3126	6	104	66	21.8	13
10647 ^a	33	842	62	21	34
69830 ^b	74	9	1900	0.02	560
			400	1.0	20
101259	30	8	271	0.98	6.0
105912	16	29	110	7.7	7.9
207129 ^c	24	274	72	15.3	12

^aThis star has a known planet orbiting at 2.03 AU (Butler et al. 2006).

^bThe first line for HD 69830 here shows our naive solution for this system, based on the fluxes at 24 and 70 microns, and assuming that all of the flux arises from continuum emission. A dust grain temperature of nearly 2000 K is not sensible, though, as this is above the sublimation temperature for any reasonable dust composition. However, Beichman et al. (2005b) found that a significant fraction of the excess flux from this system appears in emission features, meaning that our continuum assumption overestimates the dust temperature (with consequences for dust distance and fractional luminosity). The second line for HD 69830 here shows the best values for these parameters from Beichman et al. (2005b) and Lisse et al. (2007), derived from more appropriate model fitting of the emission spectrum. Note that this star has three planets orbiting within 0.65 AU (Lovis et al. 2006).

^cThere is no good K magnitude available for this star,

but Kurucz model fitting clearly indicates an excess at 24 microns. The excess at 70 microns is indicated by comparison to the Kurucz model and also by the ratio F24/F70.

Note. — T_{dust} is found by fitting a black body to the measured excesses. This black body is then scaled to fit the observed fluxes, and the ratio of this scaled black body's integrated flux to the star's integrated flux gives the fractional luminosity (f_d). We solve for R_{dust} using Equation 1. ϵ Eri is not listed here, but does have excess at both bands (Backman et al., in prep.) and a planet orbiting it (Hatzes et al. 2000).

Table 6. Dust properties for systems with excess at 70 microns only

Name	Teff (K)	Tdust (K)	Rdust (AU)	Max f_d $\times 10^{-5}$	Min f_d $\times 10^{-5}$
1581	6100	218	2.3	1.6	0.2
3296	6440	89	17	3.8	2.5
17925	5080	103	4.8	4.4	2.2
19994 ^a	6200	168	4.1	3.5	0.7
20807	5950	150	4.3	1.5	0.4
22484	6200	142	5.8	4.3	1.2
30495	5950	88	12	3.0	2.0
33262	6300	158	5.0	1.1	0.2
33636 ^b	6030	81	16	3.5	2.6
50554 ^c	6200	79	19	3.8	2.9
52265 ^d	6030	92	12	4.0	2.4
57703	6890	78	22	5.0	3.8
72905 ^{d e}	5900	123	6.2	1.5	0.6
75616	6440	77	24	3.4	2.6
76151 ^f	5830	120	5.9	1.0	0.4
82943 ^g	6030	69	22	10.0	8.8
110897	6030	94	12	2.3	1.4
115617	5770	97	8.3	3.3	1.9
117176 ^h	5770	153	3.4	7.7	1.8
118972	5080	101	5.0	4.6	2.4
128311 ^{j k}	5250	106	5.1	2.7	1.3
206860 ^l	6030	124	6.6	1.5	0.6
212695	6440	75	24	6.4	5.1

^aThis star has a known planet orbiting at 1.4 AU (Mayor et al. 2004).

^bThis star has a known planet orbiting at 3.27 AU (Butler et al. 2006).

^cThis star has a known planet orbiting at 2.28 AU (Butler et al. 2006).

^dThis star has a known planet orbiting at 0.5 AU (Butler et al. 2006).

^eBeichman et al. (2006a) derive a fractional luminosity of 2.9×10^{-5} based on 70 micron photometry and IRS spectroscopy.

^fBeichman et al. (2006a) derive a fractional luminosity of 1.2×10^{-5} based on 70 micron photometry and IRS spectroscopy.

^gThis star has two known planets orbiting at 0.752 and 1.19 AU (Mayor et al. 2004; Lee et al. 2006).

^hThis star has a known planet orbiting at 0.484 AU (Butler et al. 2006).

^jBeichman et al. (2006a) found no excess for this star in IRS spectra out to 35 microns, but calculate a fractional luminosity of 2.6×10^{-5} based on 70 micron photometry (the same data that are presented here).

^kThis star has two known planets orbiting at 1.10 and 1.76 AU (Vogt et al. 2005).

^lBeichman et al. (2006a) derive a fractional luminosity of 0.7×10^{-5} based on 70 micron photometry and IRS spectroscopy.

Note. — These dust temperatures are maximum temperatures, and the distances consequently are minimum distances. Both maximum and minimum fractional luminosity (f_d) values are given; the former corresponds to the dust temperatures and radii given in this table (see text), while the latter corresponds to 50 K dust temperature solutions. These two values give the range of fractional luminosities that fit the data (see Figure 8).

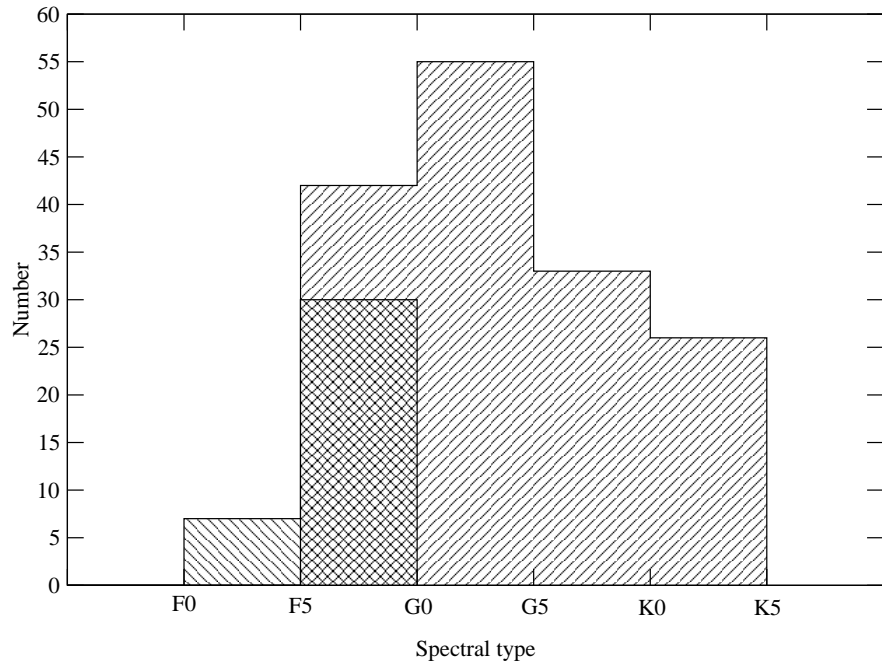


Fig. 1.— Distribution of spectral types for the 193 stars presented here. Hashes from lower right to upper left show stars from PID 30211, and hashes from lower left to upper right show stars from PID 41. Most of the targets in PID 30211 are F5 stars (difficult to see in this representation).

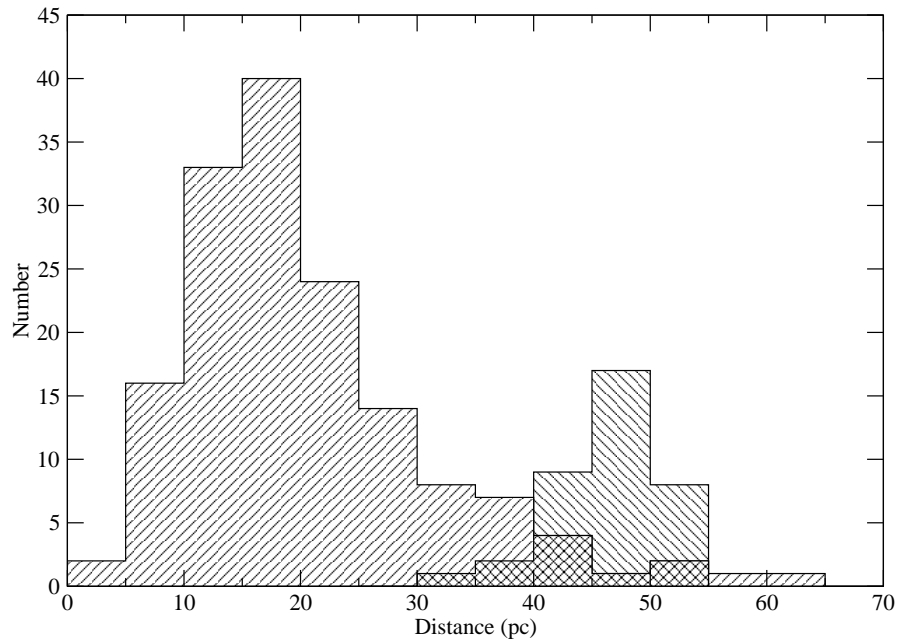


Fig. 2.— Histogram of distances for the 193 stars presented here. Three stars from PID 41 have distances off this plot: two around 100 pc, and one around 150 pc (Table 1). As in Figure 1, hashes from lower left to upper right show stars from PID 41, and hashes from lower right to upper left show stars from PID 30211.

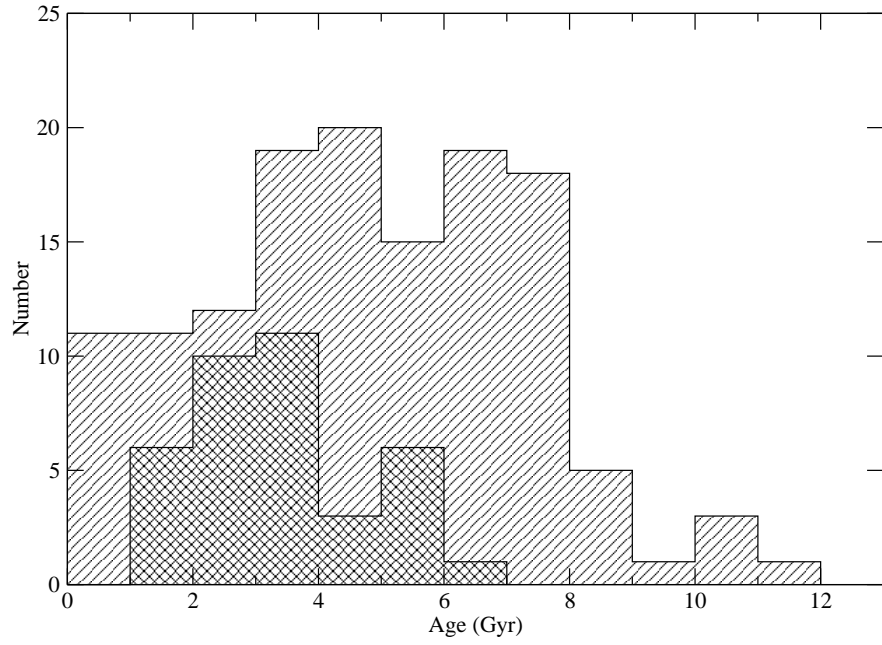


Fig. 3.— Histogram of ages for the 193 stars presented here. As in previous figures, hashes from lower left to upper right show stars from PID 41, and hashes from lower right to upper left show stars from PID 30211.

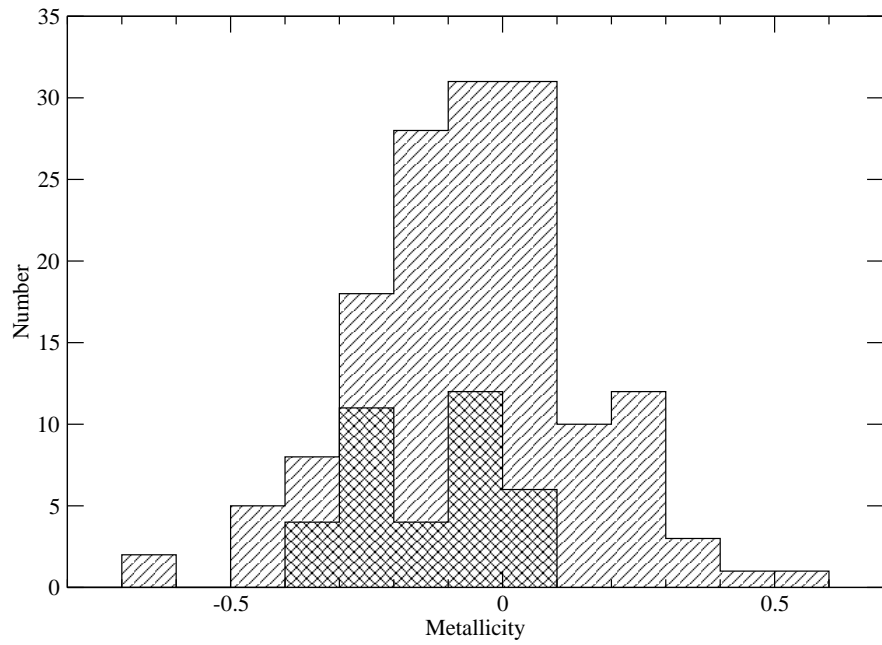


Fig. 4.— Metallicities for the 189 stars presented here with known metallicities (see Table 1). As in previous figures, hashes from lower left to upper right show stars from PID 41, and hashes from lower right to upper left show stars from PID 30211.

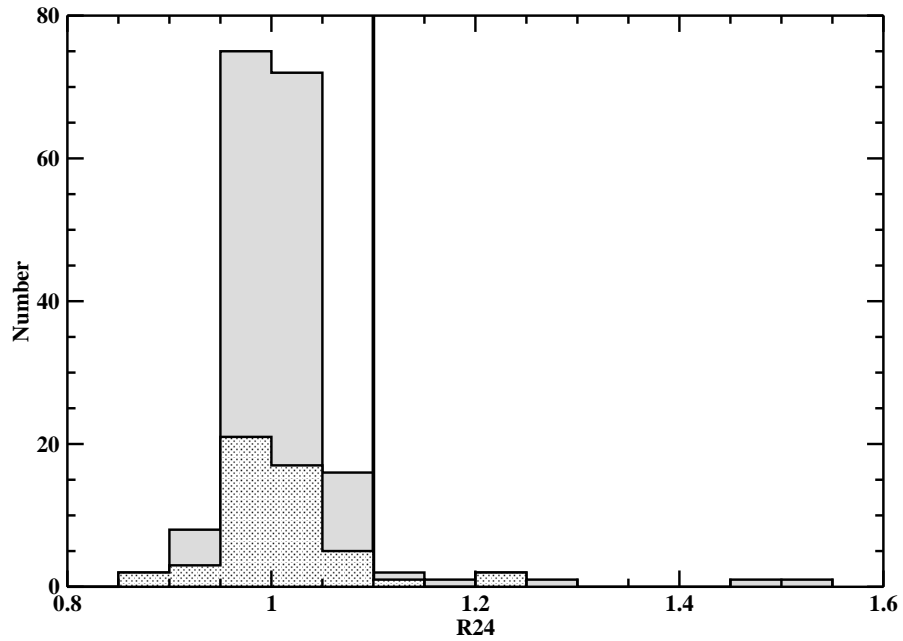


Fig. 5.— Histogram of R24 values, as described in the text. The shaded histogram shows the total number of stars in each bin, while the dotted region shows the subset for which K magnitudes are not derived from 2MASS. There is no systematic effect by using K magnitudes from other sources. The vertical line at 1.10 shows our excess threshold, as defined in the text. The core of this distribution is symmetric about unity. Seven systems have R24 values greater than 1.10; one of these is spurious, but the others are real excesses. See text for discussion.

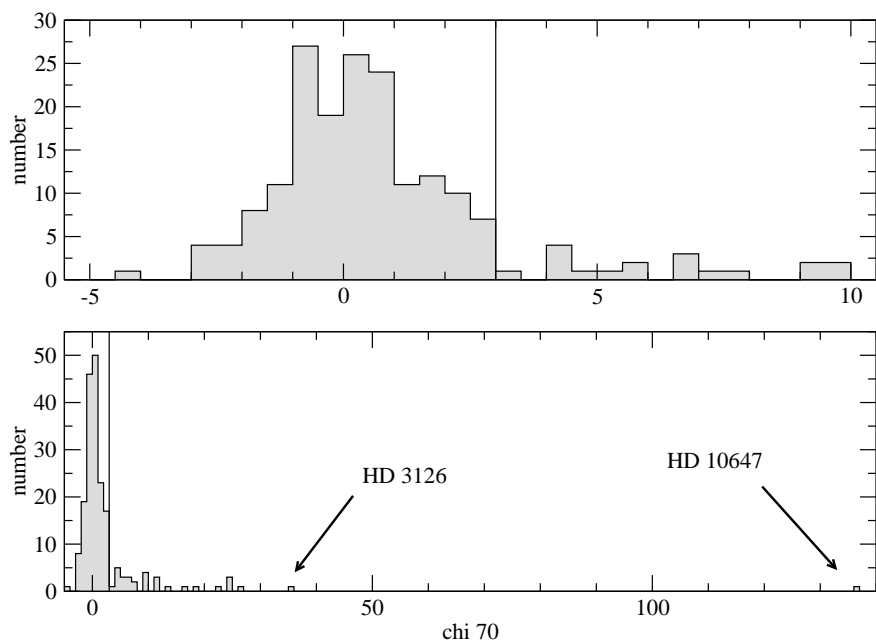


Fig. 6.— Distribution of χ_{70} values. The same data are presented in both panels. The top panel shows a smaller range in χ_{70} in order to show the shape of the core of the distribution. The lower panel shows data for all 193 systems. Vertical lines in each panel show $\chi_{70} = 3.0$, our threshold criterion. The bin sizes in the two panels are not the same (0.5 and 1 in top and bottom, respectively). Two noteworthy systems are labeled in the lower panel. The two “no K” systems HD 19994 ($\chi_{70} = 4.25$) and HD 207129 ($\chi_{70} = 24.6$) are included in this figure. HD 100067 has a very low χ_{70} value of -4.43, a result of a negative F70 value for this star, which means that this star was not detected. No stars that were detected have $\chi_{70} < -3.0$.

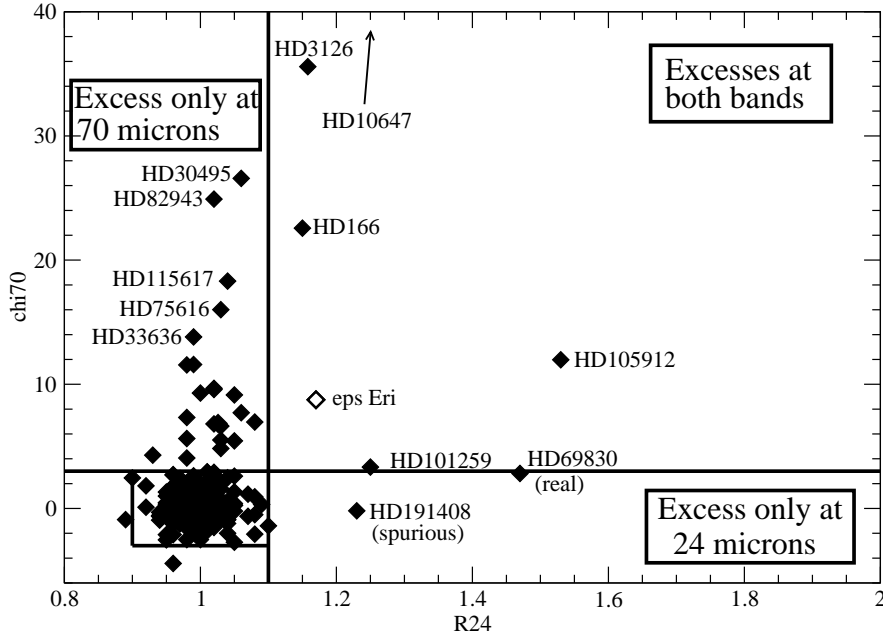


Fig. 7.— R_{24} and χ_{70} for the 181 stars with P24 (Table 3). The R_{24} and χ_{70} excess thresholds are shown by vertical and horizontal lines, respectively. The box in the lower left shows the area enclosed by $(-3\sigma, 3\sigma)$ in the two dimensions. Targets within this box show the core of our sample, having no excess at either band. In addition to showing the distribution of our sources in this parameter space, we also confirm here that no obvious systematic effects derive from our technique for deriving P24 and P70 exist. Such a systematic error would be manifest as a correlation between R_{24} and χ_{70} in the (core) non-excess sample (if the photospheric models were incorrect, for instance). Instead, we see that this core distribution is essentially a random scatter distribution (fully uncorrelated), confirming that our technique for predicting the 24 and 70 micron fluxes is appropriate. The regions with excesses at 24 only, 70 only, and at both bands are labeled. Targets with excesses at both bands are labeled (HD 10647 is off the plot to the top). HD 191408 clearly shows no excess at 70 microns, and we find that its 24 micron excess is spurious (see text). No other 24 micron excesses are spurious, since all of the rest have clear 70 micron excesses as well (excepting HD 69830, though the excess around that star is clear for many other reasons; see text). We also label the other five systems with the largest χ_{70} values. ϵ Eri (not observed as part of the programs presented here; see Backman et al. (in prep.)) is also plotted and labeled; it is clear that neither the 24 or 70 micron excesses for this famous debris disk are remarkably large. The star’s proximity (3.2 pc) accounts for its disk’s brightness and prominence.

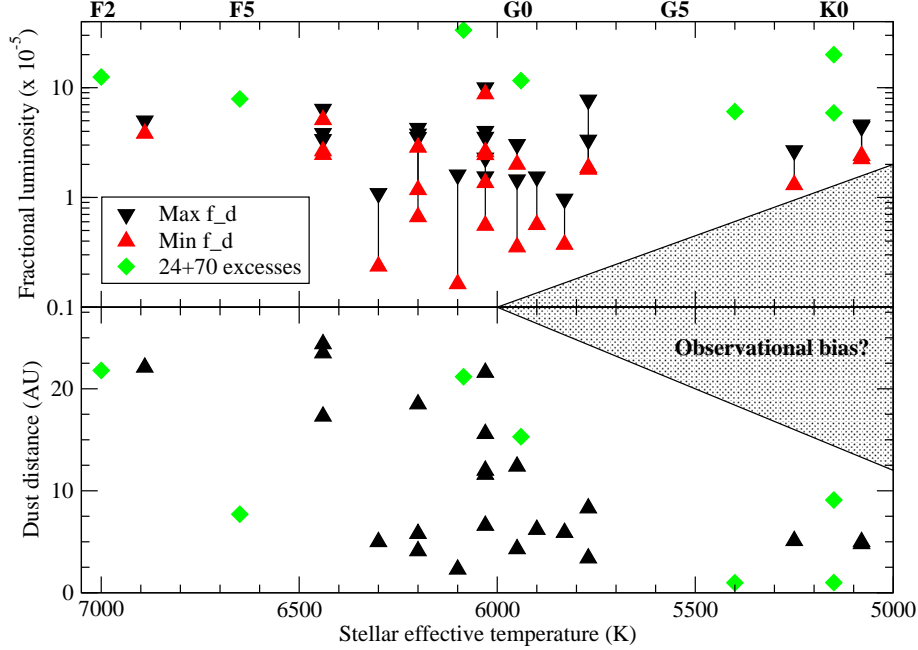


Fig. 8.— Derived fractional luminosities and dust distances as a function of stellar effective temperature (i.e., spectral type). We show maximum (downward triangles) and minimum (upward triangles) fractional luminosities in the top panel, and minimum dust distances (upward triangles) in the lower panel. For the seven systems with excesses at both wavelengths we can solve for the fractional luminosity and dust distance exactly (not limits), so these values are shown as diamonds (green symbols). These seven systems have relatively high fractional luminosities. For HD 69830, we plot here the published values from Beichman et al. (2005b) and Lisse et al. (2007). As a point of comparison, our Solar System’s asteroid belt resides at 3–5 AU, and our Kuiper Belt exists at 30–50 AU. The lack of excesses at large distances and small fractional luminosities around the latest stellar types may be an observational bias.

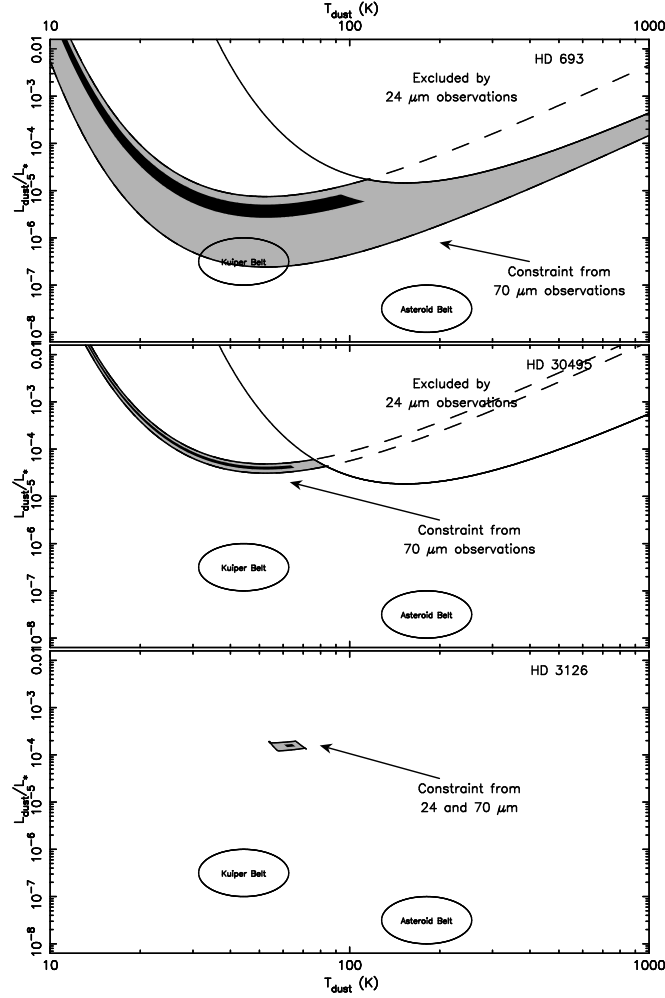


Fig. 9.— Range of possible fractional luminosities as a function of dust temperature for three noteworthy systems. The top right of each panel (hot, bright emission) is generally ruled out by our 24 micron measurements. Submillimeter observations could place limits on the top left of each panel (bright, cold emission). Based on the measured 70 micron excess, possible dust temperatures and luminosities are shown as shaded regions (gray for 3σ error limits, black for 1σ limits). The approximate characteristics of the asteroid and Kuiper belts are shown for comparison. The plausible range of dust properties for HD 693 overlaps with the properties of the dust in our Kuiper Belt (e.g., Teplitz et al. (1999)). The dust properties for HD 3126 are well-constrained due to its detection at both 24 and 70 microns.

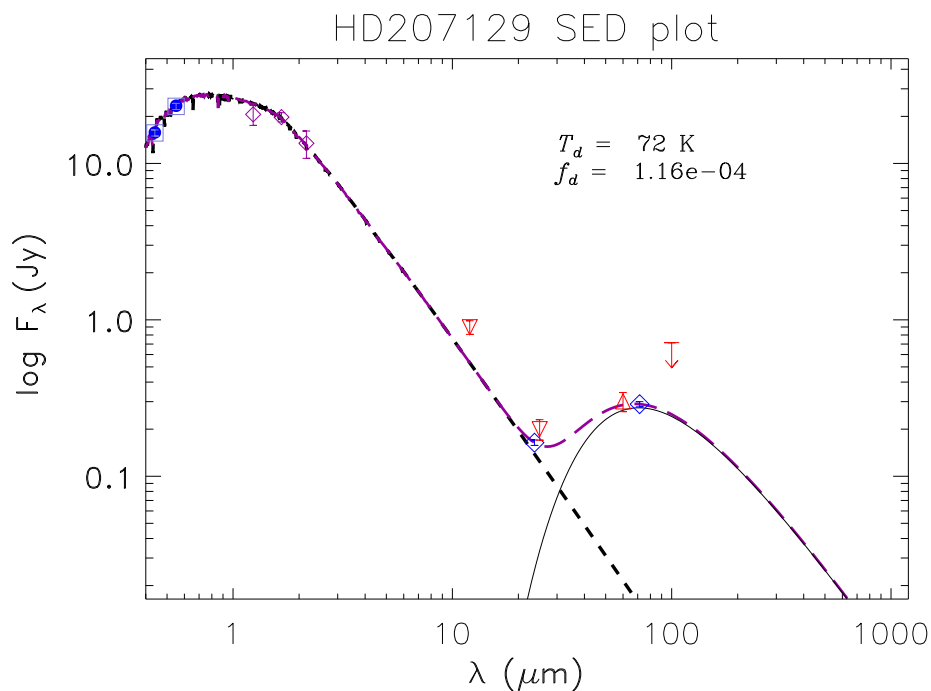


Fig. 10.— Spectral energy distribution (SED) for HD 207129. The total SED is shown by the dashed purple curve; the components are stellar (black dashed line) and dust (solid black line) emission. There is no good K magnitude for this star (the 2MASS K band error is large), but we can find a satisfactory Kurucz fit, as shown. Visible (Hipparcos) and near infrared (2MASS) photometry are shown as blue circles and purple diamonds, respectively. IRAS measurements are shown as red symbols. Our MIPS photometry is shown as blue diamonds. We find an excess at both 24 and 70 microns and therefore derive the temperature and fractional luminosity given in the legend. The high IRAS 25 micron flux is due to another bright source ~ 30 arcsec away.

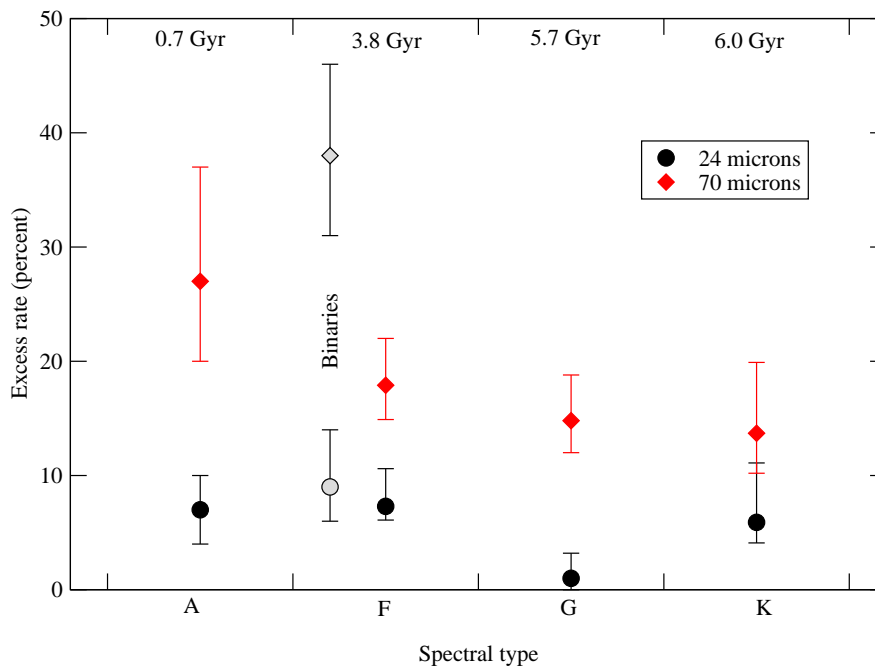


Fig. 11.— Excess rate as a function of spectral type (for “old” stars, >600 Myr). The A stars values are from Su et al. (2006) and the binaries values are from Trilling et al. (2007) (a study of debris disks in A3–F8 binaries; different shading is used here to emphasize that the sample is defined differently, i.e., includes multiplicity as a requirement). The F, G, and K samples are the union of the data presented here and in Beichman et al. (2006b). The mean ages for each of the A, F, G, and K samples are given at the top of the figure (each value has a large standard deviation of perhaps 2–3 Gyr; additionally, ages are notoriously hard to derive for main sequence FGK stars). While formally these data are consistent with no dependence on spectral type, a decrease in excess as a function of spectral type is weakly suggested. However, this could easily be an age effect (see text and Figure 12). The excess rate for (presumably old) M stars is 0%, with upper limits (binomial errors) of 2.9% at 24 microns and 12% at 70 microns (Gautier et al. 2007) (Table 4).

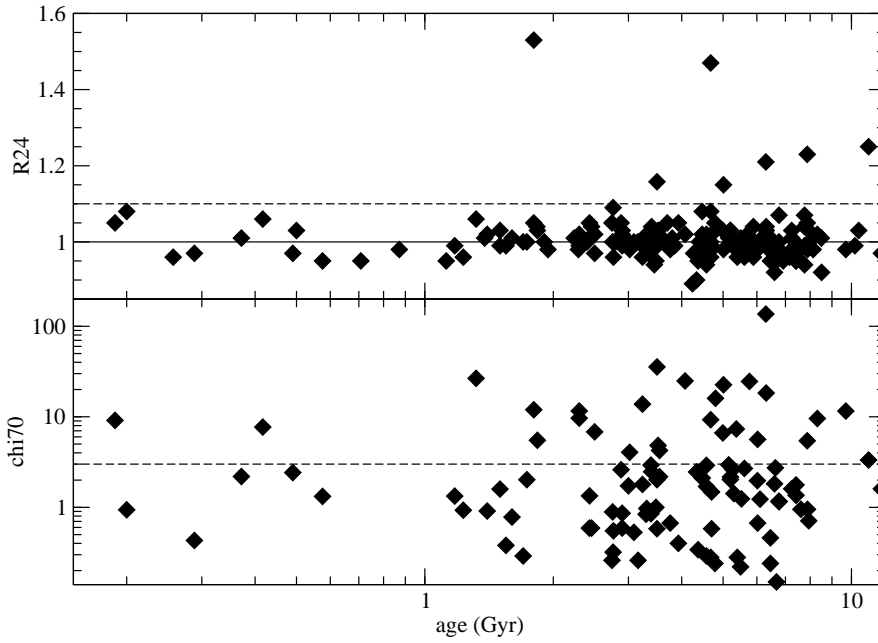


Fig. 12.— Individual R_{24} and χ_{70} determinations as a function of age for all stars in our FGK sample with good ages (164 have good ages and K band photometry and therefore R_{24} measurements; 175 have good ages and χ_{70} measurements). No trend is apparent. The solid horizontal line in the top panel indicates $R_{24}=1.0$, where there is no excess. (The no excess case in the bottom panel would be $\chi_{70} = 0.0$, which cannot be displayed on this logarithmic scale.) The horizontal dashed lines indicate our thresholds for excess ($R_{24}=1.10$ and $\chi_{70} = 3.0$).

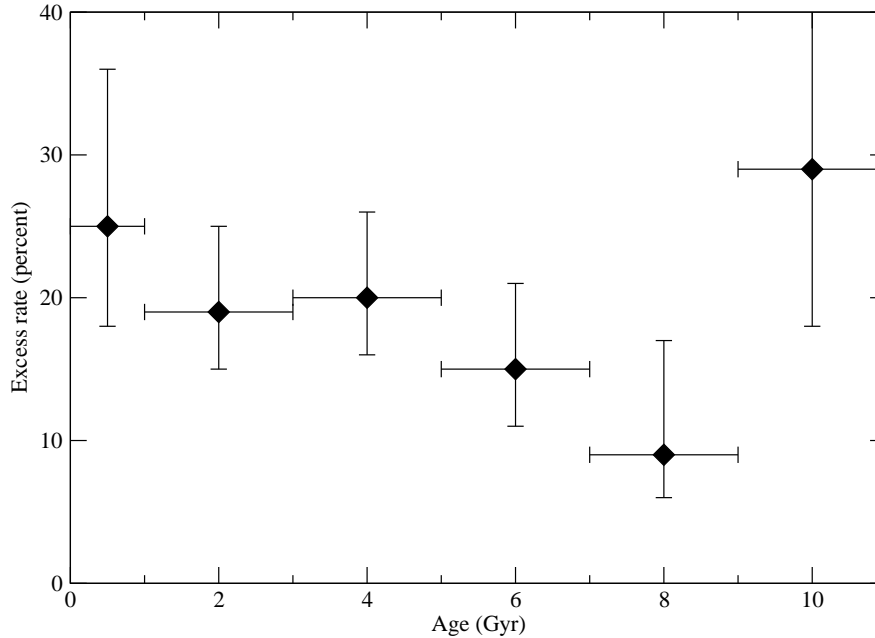


Fig. 13.— Excess rate as a function of age for the F0–K5 sample (our data plus that from Beichman et al. (2006b)). The horizontal error bars show not the uncertainties in stellar age (which could be large) but rather the bin widths. The data could be consistent with essentially no trend as a function of age (that is, with one point low and another point low), but are suggestive of an overall decrease with age. This could indicate that debris disks continue to evolve even on billion-year timescales. However, this trend could also be a manifestation of the stellar components of these bins, since the older bins will be increasingly dominated by K stars (see Figure 11). The number of stars in the six bins are as follows, from youngest to oldest: 24, 57, 60, 52, 33, 7. Since the oldest bin has only 7 stars in it (2 with excesses), the high value may be a small number statistical anomaly.

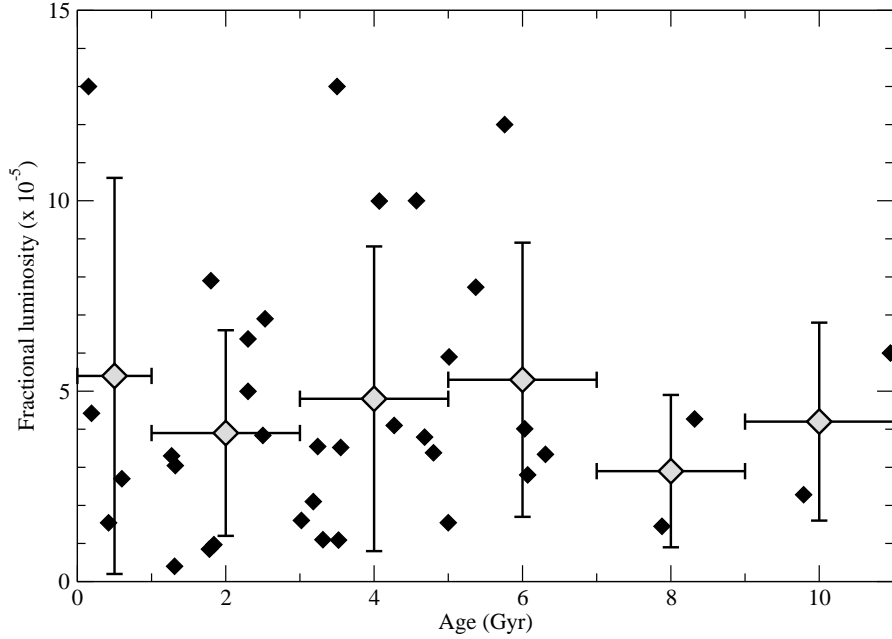


Fig. 14.— Fractional luminosity as a function of age for the excesses in the “all FGK” sample (our data plus that from Beichman et al. (2006b)). The individual data points show fractional luminosity determinations from Tables 5 and 6 (using the maximum fractional luminosity values for the 70 micron excesses only cases). The larger grey symbols show the means in the same age bins as used in Figure 13. The horizontal error bars show the bin widths, and the vertical error bars show the 1σ errors on the means. There is no obvious trend of fractional luminosity with age, though there is a lack of high fractional luminosity disks older than 6 Gyr. The systems with the three largest fractional luminosities have been omitted: ϵ Eri (0.3 Gyr, 29), HD 69830 (4.7 Gyr, 20), and HD 10647 (6.3 Gyr, 34) (where the fractional luminosities are given in units of 10^{-5}). Including these three obvious bright outliers does not change the result that no trend is evident, and just produces much larger error bars on the mean values. Our Sun has an age of 4.5 Gyr, and our Solar System’s fractional luminosity is 10^{-6} – 10^{-7} .